"DEVELOPMENT OF NANOMATERIAL MODIFIED FLEXIBLE BIOSENSOR TOWARDS POINT OF CARE DIAGNOSTICS"

A DISSERTATION

SUBMITTED IN PARTIAL FULFILMENT OF THE REQUIREMENTS

FOR THE AWARD OF THE DEGREE

OF

MASTER OF TECHNOLOGY

IN

BIOMEDICAL ENGINEERING

Submitted by

AKANKSHA

(2K16/BME/01)

Under the supervision of

PROF. BANSI. D. MALHOTRA

DEPARTMENT OF BIO-TECHNOLOGY

Delhi Technological University

(Formerly Delhi College of Engineering)

Bawana Road, Delhi-110042

JULY, 2018

DEPARTMENT OF BIO-TECHNOLOGY

DELHI TECHNOLOGICAL UNIVERSITY

(Formerly Delhi College of Engineering)

Bawana Road, Delhi-110042

DECLARATION

I AKANKSHA, 2K16/BME/001 student of M.Tech (Biomedical Engineering), hereby declare that the project Dissertation titled "Development of Nanomaterial modified flexible Biosensor towards Point of Care Diagnostics" which is submitted by me to the Department of Biotechnology, Delhi Technological University, Delhi in partial fulfillment of the requirement for the award of the degree of Master of Technology is original and not copied from any source without proper citation. This work has not previously formed the basis for the award of any degree, Diploma Associateship, Fellowship or other similar title or recognition.

Place: Delhi

Date: **AKANKSHA**

DEPARTMENT OF BIO-TECHNOLOGY

DELHI TECHNOLOGICAL UNIVERSITY

(Formerly Delhi College of Engineering)

Bawana Road, Delhi-110042

CERTIFICATE

I hereby certify that the project dissertation titled **Development of Nanomaterial modified flexible Biosensor towards Point of Care Diagnostics"** which is submitted by **Akanksha, (2K16/BME/001) [Department of Biotechnology], Delhi TechnologicalUniversity, Delhi** in partial fulfillment of the requirement for the award of degree of Master of Technology, is a record of the project work carried out by student under my supervision. To the best of my knowledge this work has not been submitted partially or fully for any Degree or Diploma to this University or elsewhere.

Place- Delhi **(Prof. Bansi D. Malhotra)**

Date- **SUPERVISOR**

ABSTRACT

We report results of the studies related to the fabrication of a novel, flexible, label-free, low-cost transducer platform comprising of Molybdenum disulfide, a transition metal dichalcogenide hydrothermally synthesized on a Whatman-1 filter paper. The obtained conducting paper has been employed for the detection and monitoring of HER-2, a widely used breast cancer biomarker. Monoclonal anti-HER-2 antibodies are immobilized via physisorption on the surface of the obtained transducer platform and BSA is then used to block the non-specific active sites, thereby producing the BSA/Anti-HER-2/MoS_2/Cellulose immunoelectrode. The structural and morphological characteristics of the fabricated composites have been studied via XRD (X-ray diffraction), FT-IR (Fourier transform infrared spectroscopy) and FESEM (Field emission scanning electron microscopy) and AFM (Atomic force microscopy) studies. Further elemental and nd electrochemical studies have been performed using UV visible spectroscopy, XPS (X-ray photoelectron spectroscopy) and Chronoamperometry studies. The electrochemical sensing studies performed on the BSA/Anti-HER-2/MoS_2/Paper immunoelectrode revealed that the proposed biosensor can detect HER-2 over a wide linear range (0.1-500 ng ml^{-1}), with an appreciable sensitivity of 78 μA ml ng^{-1} cm^{-2} and a lower detection limit of 0.07 ng ml^{-1}. Hence, this paper based biosensor is a promising alternative to conventional medical diagnostics of breast cancer due to combined advantages of the cellulose substrate such as being eco-friendly, biodegradable, low cost, flexible, foldable, lightweight and having a shorter fabrication time. Thus, our proposed biosensor offers exciting opportunities for future Point-of-Care diagnosis and monitoring of breast cancer development.

ACKNOWLEDGEMENT

I would like to express my heartfelt gratitude to my supervisor and mentor, **Prof. Bansi D. Malhotra** who has guided me through thick and thin. Without his valuable guidance, incessant help, calm endurance, constructive criticism, and constant encouragement the completion of this minor project would have been impossible, the congenial discussion with him made me confident and gave enough independence in performing the experiment which enabled in me a higher efficiency to complete the work.

I express my kind regard and gratitude of **Prof. Jai Gopal Sharma** (HOD, Department of Biotechnology), and all the other faculty members. I am highly indebted to **Ms. Shine Augustine** (Research Scholar) and **Ms. Sharda** (Post-Doctoral fellow), for their guidance and constant supervision as well as for providing necessary information regarding the instruments and experiments and also for their support in completing the reports. I am highly grateful to Nano-bioelectronics lab members for their valuable suggestion and guidance during my dissertation work. I would also like to thank **Mr. Chhail Bihari** and **Mr. Jitender Singh** for providing necessary and maintaining laboratory in good condition.

At last but never the least, words are small trophies to express my deep sense of gratitude and affection to my loving friend and my parents who gave me infinite love to go for this achievement.

AKANKSHA

2K16/BME/001

LIST OF TABLES

LIST OF FIGURES

List of Abbreviations

EIS	Electrochemical Immunosensors
AFM	Atomic Force Microscopy
CA	Chronoamperometry
CV	Cyclic Voltammetry
DPV	Differential Pulse Voltammetry
LOC	Lab-on-chip
POC	Point-of-care
PON	Point of need
SEM	Scanning Electron Microscopy
TEM	Transmission Electron Microscopy
XRD	X-ray Diffraction
PEG	Poly ethylene glycol
EDA	Ethylenediamine
TMDCs	Transition metal dichalcogenides
FEG	Field emission gun
GO	Graphene oxide
rGO	Reduced graphene oxide
MIP	Molecular imprinting polymer
ATP	Adenosine triphosphate
Human IgG	Human Intravenous Gamma Globulin
CA 15-3	Cancer antigen 15-3
AFP	α –fetoprotein
CEA	Carcinoembryonic antigen

CA 125	Cancer antigen 125
CA 199	Cancer antigen 199
PSA	Prostate-specific antigen
HCG	Human chorionic gonadotrophin
2,4-D	2,4-Dichlorophenoxyacetic acid
ECL	Electrochemiluminescence
EC	Electrochemistry
PEC	Photoelectrochemistry
FL	Fluorescence
CL	Chemiluminescence
ECL	Electrochemiluminescence
EC	Electrochemistry
PEC	Photoelectrochemistry

CHAPTER-1

INTRODUCTION

Paper has been playing a major role as a supporting material/substrate since ages. It can also act as a growth matrix for the development of coatings/thin films to realize a wide spectrum of economical applications. The advantage of paper over other conventional substances as a supporting material is its highly interconnected, macroporous and superhydrophilic structure with substantial environmental stability. Further paper displays capillary (wicking) action in the presence of hydrophilic solutions. This property can be effectively utilized for quick and uniform absorption of these solutions as pre-treatment procedures for modification of the paper substrate. Moreover, the use of cellulose as an effective substrate material for the in-situ growth of nanomaterials has gained immense attention since the past few years. The interconnected, mesh-like network of paper with high porosity between its fibers enhances diffusion of ionic species to/from the paper based electrode surface and hence boosts the electrochemical activity of the nanomaterial modified paper composites/blends.

Research in nanomaterials has been rapidly expanding over last decades due to their unique optical, electrical and mechanical. Their high surface to volume ratio provides a high surface reactivity, making them suitable for a range of applications such as supercapacitors, molecular targeting probes, drug delivery units, wearable sensors etc the nanomaterial modified paper electrodes are vastly exploited in the field of biosensing where sensing response is evaluated based on their electrochemical response studies. [36] Its because of this exciting combination of enhanced electrochemical characterstics, intrinsic mechanical flexibility, large specific surface area that paper based biosensors are in high demand these days. [37] Further, the strong hydrophilic adsorption and wicking properties of paper makes it an ideal antibody immobilization matrix. [38] Towards this objective, transition metal dichalcogenides, especially MoS_2 has stimulated much interest as the nano-transducer platform in modified paper based electrochemical sensors. [39] It is an indirect band gap semiconductor with an energy

gap of 1.2eV in bulk forms, but it gets converted into a direct band gap semiconductor as a result of quantum confinement (i.e nanoscale), which thereby increases its band gap to 1.9 eV. [40] This property of nanostructured MoS2, makes it an attractive material in the field of optoelectronics. TMDC nanomaterial generally have numerous applications such as in high-density batteries, solid lubricants, electrocatalysts, solar energy cells etc. [1–3]. Naturally, MoS_2 is found to have a hexagonal structure where individual S−Mo−S moieties interact with each other via weak Van der Waals forces. It has also got a special layered structure in which Mo and S atoms are bound by strong ionic interactions. These layers are further stacked together under the weak Van der Waals interactions to form a two-dimensional nanostructure along with its bulk counterparts. MoS_2 being a natural lubricant, its coefficient of friction is very low which has a very long life- time in vacuum and dry air environments. [4] Nanostructured MoS_2 has been synthesized by a number of methods such as gas-phase method, hydrothermal method, laser ablation, thermal decomposition and sono-chemical processes. Using these methods, its different morphologies can be prepared such as nanotubes, nanowires, nanorods, nanosheets and nanoflowers. [5-8] MoS_2 has got a higher environemtal stability due to intrinsic disulfide linkages along with good optoelectronic properties due to its band gap tunability (based on the number of MoS_2 layers in a nanostructure). Thus, 2D nanomaterials have got promising potential to replace the established graphene based devices in the near future making them excellent candidates in electrochemical appplications, which were earlier dependent on graphene. Development of paper based biosensors extends their scope to wearable sensors for personalized diagnostic and continous health montitoring. Further, cellulose is found to be highly stable in most solvents and is both hydrophilic and lipophilic, making it versatile to use in a variety of reaction environments In this work, a nanostructured MoS_2 modified paper based electrode have been fabricated for electrochemical biosensing of breast cancer biomarkers. The MoS_2/paper composite has a porous and flexible structure with an efficient current collecting ability, optimized for its role as a POC immunosensor. This prototype has not only displayed promising potential as a future point of care diagnostic device for breast cancer detection but can also be extended to other forms of cancer detection in the near future.

CHAPTER-2

LITERATURE REVIEW

2.1 Paper

It is made up of cellulose (linear homopolymer) microfibers arranged in a random, mesh-like network consisting of β-(1,4) glycosidically linked D-glucopyranose monomers. It is the raw material for cotton fabrics (textile industry) and is said to be the most abundant natural polymer found in nature. It is easily biodegradable and hence disposable, although it has a high thermal stability. Moreover, these days cellulose based materials such as filter paper are chemically modified for various optoelectronic, electronic, electrochemical and colorimetric applications. In recent years, development of paper based flexible biosensors has increased significantly in the fields of medical diagnostics and healthcare. They not only help in disease diagnosis but also in the early diagnosis during the incubation period of a particular disease. Thus, paper based biosensors are effective point of care (POC) diagnostic devices which shall play a vital role in health monitoring and hence they are in global demand. They are important for low and middle-income countries, which are already lacking infrastructure and are financially weak and also in such countries with high chances of a breakout of endemic infections. The demand of point of care diagnosis worldwide is not only for advancements in theranostics and personalized medicine but worrying global population trends such as ageing population in the developed countries, population explosion in developing countries etc. This called for the need of cheap and rapid tests which would not only be environment friendly but would also be user friendly. Thus, it lead to the development of point of care diagnostic testing devices (POCTs) to initiate a new wave of personalized healthcare. Further, cellulose paper has been found to be an ideal substrate for diagnostic devices as its fiber act as a passive support for mediating the faster and efficient interaction of the analyte with the sensing element and the signal produced from the interaction is then detected by the chosen transduction pathway. In this work, a novel, conducting, flexible MoS_2-paper composite has been synthesized by

the hydrothermally-assisted growth of an MoS_2 coating on the surface of cellulose fibers. It is the capability of cellulose fibers to control the nucleation rate, which makes uniform growth of the MoS_2 nanostructures possible on their surface. Therefore, by using the polyol nature of cellulose fibers it is possible to uniformly absorb the seed solution and ultimately control the rate and quantity of MoS_2 nanostructure nucleation. Also, the reaction of precursors i.e. l-cysteine and sodium molybdenum hydrate is said to be highly specific to their interaction with the functional groups and ions present on the surface of the cellulosic matrix which dictates the morphology and crystallinity of the resultant MoS_2 nanostructure.

2.1.1 Advantages of using a Paper based substrate

Paper being lightweight, affordable, portable, easy to use, flexible, biodegradable and disposable fulfills the preliminary requirements for the development of a point of care (POC) biosensor, enabling the growth of nanomaterials on its surface for low cost device fabrication. It generally degrades around 300°C making it suitable for most low temperature experimental processes. Therefore, we have exploited these advantages of paper while fabricating a flexible, portable and disposable biosensing platform to quantify the levels of breast cancer associated antigens found in human serum. The transducer platform comprises of a nanocoating of hydrophobic MoS_2 on paper which provides a favourable antibody immobilization matrix that ultimately leads to the development of an immunosensor for breast cancer biomarker detection.

Table 2.1: Nanomaterial Modified Paper based Biosensors

Nanomaterials	Analytes	Detection Methods	Linear Range	Detection Limit	References
Au + Ag	Cell	FL	80–5.0×10^7 cells ml^{-1}	26 cells ml^{-1}	10
Au + Pt	CEA AFP	PEC	1.0 pg ml^{-1} – 100 ng ml^{-1} 1.0 pg ml^{-1} – 100 ng ml^{-1}	0.30 pg ml^{-1} 0.50 pg ml^{-1}	11
Pd + Au	CEA	EC	1.0 pg mL^{-1} – 100 ng ml^{-1}	0.40 pg ml^{-1}	12
ZnO	CEA	PEC	0.001–90 ng ml^{-1}	0.33 pg ml^{-1}	13
TiO2	PSA	EC	0.3 pg ml^{-1} – 7 μg ml^{-1}	0.10 pg ml^{-1}	14
TiO2	CEA	PEC	0.001–2.5 ng ml^{-1}	0.39 pg ml^{-1}	15
ZnO	AFP	EC	0.0002–500 ng ml^{-1}	0.08 pg ml^{-1}	16
ZnO	CEA CA 125 CA 15-3	PEC	0.005–20 ng ml^{-1} 0.01–50 U ml^{-1} 0.01–50 U ml^{-1}	1.8 pg ml^{-1} 3.6 mU ml^{-1} 3.8 mU ml^{-1}	17
ZnO	H2S from cell	ECL	1000– 5.0×10^7 cells ml^{-1}		18
SnO2	ATP	PEC	0.1 pM –100 nM	0.025 pM	19
rGO	Pb^{2+}	EC	0.005–2000 nM	0.002 nM	20
rGO	HCG PSA CEA	EC	0.002–120 mIU ml^{-1} 0.001–110 ng ml^{-1} 0.001–100 ng ml^{-1}	0.0007 mIU ml^{-1} 0.35 pg ml^{-1} 0.33 pg ml^{-1}	21
GO	AFP	EC	0.001– 10 ng ml^{-1}	0.5 pg ml^{-1}	22
GO	CA 15-3	EC	10^{-3}–200 U ml^{-1}	2.8 × 10^{-4} U ml^{-1}	23
rGO	CEA	ECL	0.3 –8000 pg ml^{-1}	0.08 pg ml^{-1}	24
MIP	D-glutamic acid	EC	1.2 nM – 125.0 nM	0.2 nM	25
MIP	2,4-D	CL	5.0 pM–10.0 μM	1.0 pM	26
MIP	Heptachlor	PEC	0.03 – 10.0 nmol l^{-1}	8.0 pmol l^{-1}	27

MIP	Pentachloro-phenol	PEC	0.01–100 ng ml^{-1}	4 pg ml^{-1}	28

2.2 Transition metal dichalcogenides (TMDCs) and Biosensors

Transition metal dichalcogenides (or TMDCs) consists of a layered crystal structure in which the transition metals such as tungsten, molybdenum or niobium are linked with group 16 elements (or chalcogens) such as sulfur, selenium etc. Each layer contains repeating units comprising of a transition metal atom sandwiched between two chalcogen atoms and are held together by covalent bonds. However, neighbouring sheets interact with each other by weak Van der waals forces.

In recent years, TMDCs have been employed in various electronic and electrochemical applications by fabricating their 2-D thin films. Biosensors on the other hand employ biomolecules as the bioreceptors that recognize the target analytes and utilize a transducer platform to convert the biochemical interaction signal into an optical, electrical or calorimetric signals to determine the concentration of the target analyte. TMDCs are widely utilized in electrochemical biosensors owing to their semiconducting properties and high electrocatalytic activity. The confluence of TMDCs and electrochemical biosensors has created many productive sensing strategies for applications in many areas such as clinical diagnosis, food safety & environmental monitoring. 2D layered TMDCs such as MoS_2 exhibit a number of properties like large surface area, high surface energy, fast heterogeneous electron transfer, good electrical conductivity, field effect, quantum size effect, intercalation of atoms, ions & molecules into Van der Waal layers etc. All these properties of TMDCs makes them superior over gapless graphene, thus making it possible for 2D materials such as MoS_2 and other TMDCs to be used in the next generation optoelectronic and health monitoring devices. So far, many people have synthesized TMDCs-based nanomaterials for development and fabrication of advanced electrochemical biosensors with promising performance for various electronics and healthcare applications. Here also, a transition metal dichalcogenide (TMDC) especially MoS_2 based electrochemical immunoelectrode has been synthesized hydrothermally on the surface of cellulose paper for fabrication of an electrochemical biosensor and is proposed to detect levels of Breast cancer biomarkers in blood.

2.3 Cancer

All cells in the body have got a definite life span after which they stop performing their integrated specific functions and undergoes a self destruction mode called as apoptosis, which is in other terms knows as programmed cell death (or natural cell death). New cells then replace these dead cells and this is how the cell cycle goes on in a balanced integrated manner maintaining a fairly constant number of cells over a time span. However, due to certain reasons, such as any kind of mutation or transformation few

cells fail to follow the typical cell cycle mechanism and continue to grow indefinitely in an uncontrolled manner. These type of cells are known as immortal ones as they continue to divide rapidly into clones of abnormal cells and gives birth to a condition called as cancer and the corresponding cells are known as cancerous cells. In short cancer may be defined as the uncontrolled, rapid growth of abnormal cells that ultimately destroys body tissues. According to a report from WHO, cardiovascular reasons are the first behind most of the deaths all over the world followed by cancer. Among them breast cancer is second deadliest preceded by lung cancer. Basically all these diseases are a result of lifestyle changes and most importantly the pollution and the situation is grimmer in developed countries due to their sedentary lifestyle, greater exposure to carcinogens, increased conviction on processed foods and genetically engineered food.

2.3.1 Breast cancer

Breast cancer is a collection of tumor (or cells) that arises from the breast cells. It is the most common cancer among women and majority of these cases occur in developing countries as compared to western ones. There is an expectation of 266,120 new cases in 2018 as reported by WHO among women in Asia and 2,550 cases in men respectively. Every year nearly ~ 460 man and 40,610 women die because of breast cancer. To spread awareness among individuals, government has created many organizations. There are different types of breast cancers and their symptoms include: a change is the size of the breast, swollen lymph node in the neck, lump in the breast, bloody nipple discharge etc.

2.3.2 Conventional techniques for Breast cancer detection

Coventionally scanning of breast is performed under compression using X-rays. Thus, it has been diagnosed using various imaging techniques such as breast imaging, screen film mammography (SFM), mammography etc. It is the breast's density that affects the results of mammography which is further affected by hormones, age, BMI (body mass index), menstrual cycle phase, genetic vraiations etc. But there are certain problems and discomforts while performing mammograms such as compression of breasts makes

patients uncomfortable, requires a trained X-ray technician, and a radiologist, radiographic films and use of various developing chemicals. Also, unnecessary biopsies has to be performed after reading the images of mammograms. Computer aided detection and diagnosis (CAD) is used for identification of suspicious abnormalitoes present in the tissue images with the help of vaarious pattern recognition softwares. Software marks all the abnormal (i.e benign and malignant) tissues in the image. Further, sono- mammaography or ultrasonography (US) is performed to follow up the abnormalities seen in mammograms. Currently a handheld 1 cm by 6 cm transducer probe is used which is placed on the breast surface by a technician and moved around the breast area. Technicians label all the images w.r.t the orientation and location of the surface. Its disadvantage is the small probe size, which makes it difficult to cover the entire breast surface for screening. Compound multiple ultra-sonography is also performed to combine multiple images into one to subtract the background noise, clutter, yielding a smoother and high quality clear image. It basically performs tissue differentiation producing a more realistic image of the tissue of interest. One more technique is used to keep track of the effective blood flow called as Doppler ultrasonography. It helps in finding the origin of benign and malignant tunors. MRI or Magnetic Resonance Imaging (MRI) is also performed for obtaining spatial and temporal resolutions as it creates 2-D and 3-D images using magnetic field. Generally, a contrast agent especially gadodolium based is used for imaging purposes. Then nuclear medicine techniques such as radioimmunoscintigraphy (RIS) have been used during which the patients are exposed to radiation but then it shows promising results specially in case of high-risk patients. It basically identifies tumor-associated antigens and treats them by injecting radiopharmaceutical agents, which then results in different antigenic expression of normal and cancerous cells. Another tomography technique called as Positron emission tomography (PET) uses glucose metabolism using ^{18}F fluorodeoxyglucose (or FDG), to detect cancerous tissues. PET has been well established in detection of various types of malignancies, especially in solid organ tumors. All these techniques are time consuming, expensive and requires professional experties. Biosensors on the other hand are higly sensitive, minimally invasive, specific, they allow for personalized diagnostics and hold immense potential as point of care devices. So far, various biosensors has been developed for breast cancer detection targetting specific biomarkers during earlier stages using modified nanomaterials. A

biosensor designed for cancer diagnosis consists of a recognition element (bioreceptor), target molecule (biomarker) and a transducer. It gives quick response due to fast electron transfer rate and high electrochemical activity of the nanomaterial coating. Quantification of biomarker levels is useful for their correlation with tumor stages.

2.3.3 Biomarker

Biomarker levels signify the status of pathological or pharmacological response in the human body. These are extracellular domains shed off from the cell surface. Changes in Biomarkers are specific to progression of cancer stages. It detects physical, chemical and biological parameters and measures them in bodily fluids. They are directly associated with cells, proteins and specific biological elements. Biomarkers are useful indicators of both metabolic as well as infectious diseases. Biomarker requires bio-recognition elements for their quantification, which is based on the lock and key hypothesis. The output of the biochemical interaction is transduced by the nanotransducer MoS_2 platform. The selection of nanotransducer depends upon the interaction of biomarker with the transducer. For example, a potentiometric transducer quantifies change in proton concentration whereas; amperometric transducer quantifies change in electron concentration. Change in optical parameters such as light, transmittance, absorbance, reflectance are measured by an optical transducer and mass by piezoelectric transducers. A reasonable correlation exists between the prognostic and diagnostic values of a marker such as HER-2, estrogen and progesterone are regarded as both the markers (Misek and Kim et. al, 2011). Hence, a prototype has been designed to target the alarming rate of increase in breast cancer cases, which has been known to be one of the leading contributors of global death. Detection of a biomarker can warn us about the onset of a particular disease. Further, the point of care diagnosis could make our life much easier and stress free. Here, a flexible MoS_2 paper based composite platform has been fabricated and utilized as an antibody immobilization matrix.

Table 2.2 Normal levels of different biomarkers in Breast Cancer

BIOMARKERS	NORMAL LEVEL
CEA (Carcinoembryonic antigen)	2.5 μg l^{-1} in nonsmokers, 5 μg l^{-1} in smokers
CA15-3 (Cancer antigen 15-3)	25 kU l^{-1}
CA27.29 (Cancer antigen 27.29)	38 kU l^{-1}
CA72-4 (Cancer antigen 72-4)	7 kU l^{-1}
CA549 (Cancer antigen 549)	10 kU l^{-1}
uPA (Urokinase plasminogen activator)	198-511 μ l^{-1}
VEGFR (Vascular endothelial growth factor receptor)	15 ng l^{-1}
HER1 (Epidermal growth factor receptor)	75.3 μg l^{-1}
HER2 (Epidermal growth factor receptor)	2-15 μg l^{-1}
HER3 (Epidermal growth factor receptor)	0.06-2.5 μg l^{-1}
MUC1 (Mucin 1)	0.7-39.8 kU l^{-1}
p53 tumor suppressor protein	150 ng l^{-1}
CD146 (Cluster of differentiation 146 antigen)	309 μg l^{-1}
IL-6 (Interleukin 6)	10 75 ng l^{-1}
IL-8 (Interleukin 8)	13 ng l^{-1}
PR (Progesterone receptor)	0.6 μg g^{-1} cytosol

2.3.4 HER-2 (Epidermal growth factor receptor)

Antibodies are biopolymers with molecular mass ~150 kDa and consists of amino acid sequence which defines its three dimensional structure. It consists of two fragments namely antigen binding region and a fragment crystallizable region (Fab and Fc) respectively. The antigen binding regions which are joined together by the hinge region, are known as $F(ab)_2$ fragment. Generally, the antibody is immobilized in such a manner

that the F_c region faces the substrate. However, the conducting characteristics and small band gap of MoS_2 makes it favorable for the conduction and transfer of electrons. This miniaturized electrochemical electrode is low cost, stable, simple, reproducible, eco friendly and portable. Growth of MoS_2 on paper surface results in improved electrochemical characterstics of the breast cancer biosensor and this modified paper based electrode is used as an immobilization matrix for HER-2 antibody. Epidermal growth factor receptor or HER-2 is a proto-oncogenic glycoprotein (~185 kDa M. Wt.). It is a trans-memberane protein and is found to be overexpressed in most of the breast cancer cases i.e it is considered as one of the important breast cancer biomarker. HER-2 receptor consists of ligand binding domain in the extracellular region & a tyrosine kinase domain in the intracellular region and both these domains are responsible for cell survival, its proliferation and differentiation. As soon as ligand binds to the receptor it undergoes conformational changes resulting in dimerization of ligand binding domain and phosphorylation of tyrosine kinase domain. It is the result of proteolytic cleavage of the extracellular domain that releases cells in the blood and are detected as abnormal biomarker levels. Dimerization and phosphorylation events in turn activate the signaling cascade pathway. HER-2+ breast cancer is the most aggressive type of cancer and is very difficult to treat. In breast cancer patients, high level of HER-2 in blood is associated with less chances of survival. Thus, Anti-HER-2 has got potential applications in breast cancer patients. Generally immunotherapy with Herceptin is performed for the treatment. It is a monoclonal antibody that binds to the extracellular domain, thereby blocking the binding of ligand and inhibiting the transduction pathway. Chemotherapy or hormonal therapy is performed in response to raised levels of HER-2. Thus, to use biosensor as POCT device for breast cancer detection Anti-HER-2 is immobilized on the surface of hydrothermally synthesized MoS_2 paper substrate. The unbound antibodies are washed off with PBS (Phosphate buffer saline) and are further blocked by BSA (bovine serum albumin) protein. Electrochemical studies has been performed on the above fabricated electrode surface to measure the HER-2 concentration in the sample.

Target molecule	Biosensor specification	Linear range of detection	Detection limit	Reference

Table 2.3 Different Biomarkers for Breast Cancer Detection

BRCA1	ssDNA /PEG/GCE /AuNP	50.0 fM–1.0	1.7 fM	(Wang et al., 2015b)
	ssDNA/ RGO/ GCE/ PANHS	$10^{-18} \times 10^{-10}$ M	3.5×10^{-19} M	(Benvidi et al., 2016)
CEA	AuNPs/ZnONPs/Au electrode/ HRP/anti-CEA	0.1–70 ng ml^{-1}	0.01 ng ml^{-1}	(Norouzi et al., 2011)
	Ag/ BSA /Ab1/ Au–TiO2/ HRP-Ab2–HPtNPs	0.02–120 ng ml^{-1}	12 pg ml^{-1}	(Yang et al., 2011)
CA15–3	GCE/Pt NCs/OrgSi@CS-CNTs	0.1–160 U ml^{-1}	0.04 U ml^{-1}	(Li et al., 2010b)
VEGF	Au electrode/ Aptamer-methylene blue	50 pM–0.15 nM	5:00 PM	(Zhao et al., 2011)
EGFR	DTSP/Au electrode /EA/Anti-EGFRab	1 pg–100 ng ml^{-1}	1 pg ml^{-1}	(Vasudev et al., 2013)
	Cys/AuNPs/Au electrode/ PG/PDITC	1 pg–1 mg ml^{-1}	0.34 pg ml^{-1}	(Elshafey et al., 2013)
ER	SiNW/ERα-ERE	1 pM–10 fM	10 fM	(Zhang et al., 2011)
FA	Au electrode/ FA-Folate/DNA probe	10^2–10^6 cells ml^{-1}	67 cells ml^{-1}	(Zhao et al., 2013a)
EpCAM	Au electrode/LC-SPDP / Anti – EpCAM	1×10^5–1×10^8 cells ml^{-1}	1 10^5 cells ml^{-1}	(Arya et al., 2013)
HER-2	HER-2/Anti-HER-2/SPCE /Anti-HER-2-S-AP	15–100 ng ml^{-1}	4.4 ng ml^{-1}	(Marques et al., 2014)
	GNP@MW-CILE /Ab/GNP/HDT	10–110 ng ml^{-1}	7.4 ng ml^{-1}	(Arkan et al., 2015)
	AP-Ab2/HER-2/Anti – HER-2	0.2–2 ng ml^{-1}	0. 2 ng ml^{-1}	(Qureshi et al., 2015)
HER-2 ECD	Protein A/MB/SPE /ECD/Ab1	0–15 ng ml^{-1}	6 ng ml^{-1}	(Al-Khafaji et al., 2012)
HER-3	Anti-HER-3/HER-3/BSA/HER-3/4-ATP/Au electrode	0.4–2.4 pg ml^{-1}	0.4 pg ml^{-1}	(Sonuç and Sezgintürk, 2014)
HER-2	**BSA/Anti-HER-2/MoS_2-Paper composite**	**0.1-500 ng ml^{-1}**	**0.07 ng ml^{-1}**	**THIS WORK**

2.4 Flexible paper based biosensors

Xie et. al, 2016 fabricated carbon based MoS_2 eletrode for sodium-ion batteries by hydrothermal synthesis method by performing carbonization of paper towel followed by deposition of MoS_2, which were reported to align vertically on carbon scaffolds.Cyclic performance of as prepared electrodes were improved by dip-coating with carboxy methyl cellulose. As a result the electrodes exhibited high reversible capacity, high initial coulombic efficiency and promising rate capability. Sahatiya et. al, 2017 developed a 2-dimensional MoS_2-CQD (Carbon quantom dot)based flexible broadband photodetector where MoS_2 was grown on cellulose paper by hydrothermal treatment and CQD was fabricated using chia seeds by one step pyrolytic process. Differences observed in fermi levels of CQD and MoS_2 created a unipolar junction. This junction then created a local electric field, which upon illumination in UV visible and NIR, separated charge effectively. Responsivity results were showig that the as fabricated photodetector was more responsive towards visible light as compared to UV and NIR. Gomathi et. al, 2017 fabricated a ZnS- MoS_2 based flexible broadband photodetector on cellulose paper by hydrothermal method. The sensitivity of photodetector when compared to UV and IR was high for visible light. ZnS- MoS_2 pair shows increased responsivity due to their reduced electron-hole recombination. ZnS was responsible for formation of local electric fields and also for the absorption in UV range. The as fabricated low-cost, paper based flexible photodetector provides promising applications in the field of wearable electronics, surveillance and environmental monitoring. Sahatiya et. al, 2017 developed a flexible piezotronic diode based on MoS_2-CuO using hydrothermal method, which upon external strain acted as analog frequency modulator and enhanced broadband photodetector. Further, the applied external strain in the fabricated piezotronic diode was used as a frequency controller for designing an oscillator. This work demonstrated tremendous potential at circuit level designing in the field of wearable sensors, digital and electronics applications. Sahatiya et. al, 2017 demonstrated a two dimensional Gr/ MoS_2 photodetector on cellulose paper by hydrothermal method followed by assembly on PDMS substrate. Gr was responsible for charge transport layer and MoS_2 for absorption process. Enhanced photosensing of visible and IR light was observed under 2% strain and this was due to the potential barrier strain between MoS_2 and Gr and a negative piezopotential that developed in MoS_2. As a result conduction band energy was reduced increasing the barrier potential thus efficiently separating electron-hole pair. The work is providing promising applications for development of large area flexible paper based broadband

photodetectors at low cost using Gr/ MoS_2 in the field of wearable, digital and analog electronics. Sahatiya et. al, 2018 used different flexible substrates (like cellulose paper, ceramic paper, carbon paper, Silicon cloth, thread, aluminum foil, copper foil and polyimide) for growth of MoS_2 using hydrothermal method at 200^0 Celsius. Providing similar hydrothermal conditions, they observed morphologies of MoS_2 at different flexible substrates. They demonstrated that substrate was found to have an effect on number of layers and defects of MoS_2. Also, they explained kinetics of growth using growth theory, classical nucleation and surface energy of substrate. Further, photodetection studies revealed that the defects introduced in the hydrothermal process were playing an important role in photodetection. Their work finds potential applications in energy storage, electronics, optoelectronics, and acts as a substitute for conventional CVD processes used for the growth of MoS_2. Sahatiya et. al, 2018 fabricated first time, Al foil as electrode on hydrothermally synthesized MoS_2 paper. Here, cellulose paper was used as dielectric and they were able to change the capacitance of as fabricated flexible capacitor by applying the external mechanical strain. The strain applied here was directly proportional to the capacitance of flexible MoS_2 capacitor and inversely proportional to the frequency of oscillator. The effect of strain on the parameters of the filter circuit such as, cut off frequency, gain, phase and time constant were studied. Then, movement of fingers was finally integrated with the flexible MoS_2 capacitor suggesting its application in human motion monitoring systems. Their work is a suggestive of simple and low cost, wearable capacitors for the applications in the field of flexible electronics holding tremendous potential in personal healthcare monitoring. Wang et. al, 2018 developed a novel active and flexible electrochemical sensing platform of freestanding graphene paper supported MoS_2 nanocrystals monolayer with Cu submicron buds for glucose and lactate detection for the first time. The strategy has several advantages, including the following: (i) The use of freestanding graphene paper enable facile assembling of the active components, 3D Cu submicron- buds and monolayer of 0D MoS_2 nanocrystals, and gives rise to impressive flexibility and lightweight of the biosensors; (ii) The synergistic effect between MoS_2 nanocrystals and Cu submicron-buds along with the immobilization of lactate oxidase boost electrochemical sensing performances enables bio-functional detection of glucose and lactate to integrate into one platform, which simplifies the measurement process; (iii) The 0D MoS_2 nanocrystals monolayer supported 3D Cu submicron- buds possess high electrocatalytic activity toward glucose and lactate in human perspiration,

which provides new insight into the design of non- noble metals electrodes for sweat glucose and lactate monitoring. As a result, this electrochemical biosensing platform of high flexibility and sensitivity, low cost, as well as facile fabrication is believed to possess potential opportunities for using as key component in new generation of wearable sensors, implantable biomedical devices and potable diagnostic electronics.

CHAPTER-3

OBJECTIVES

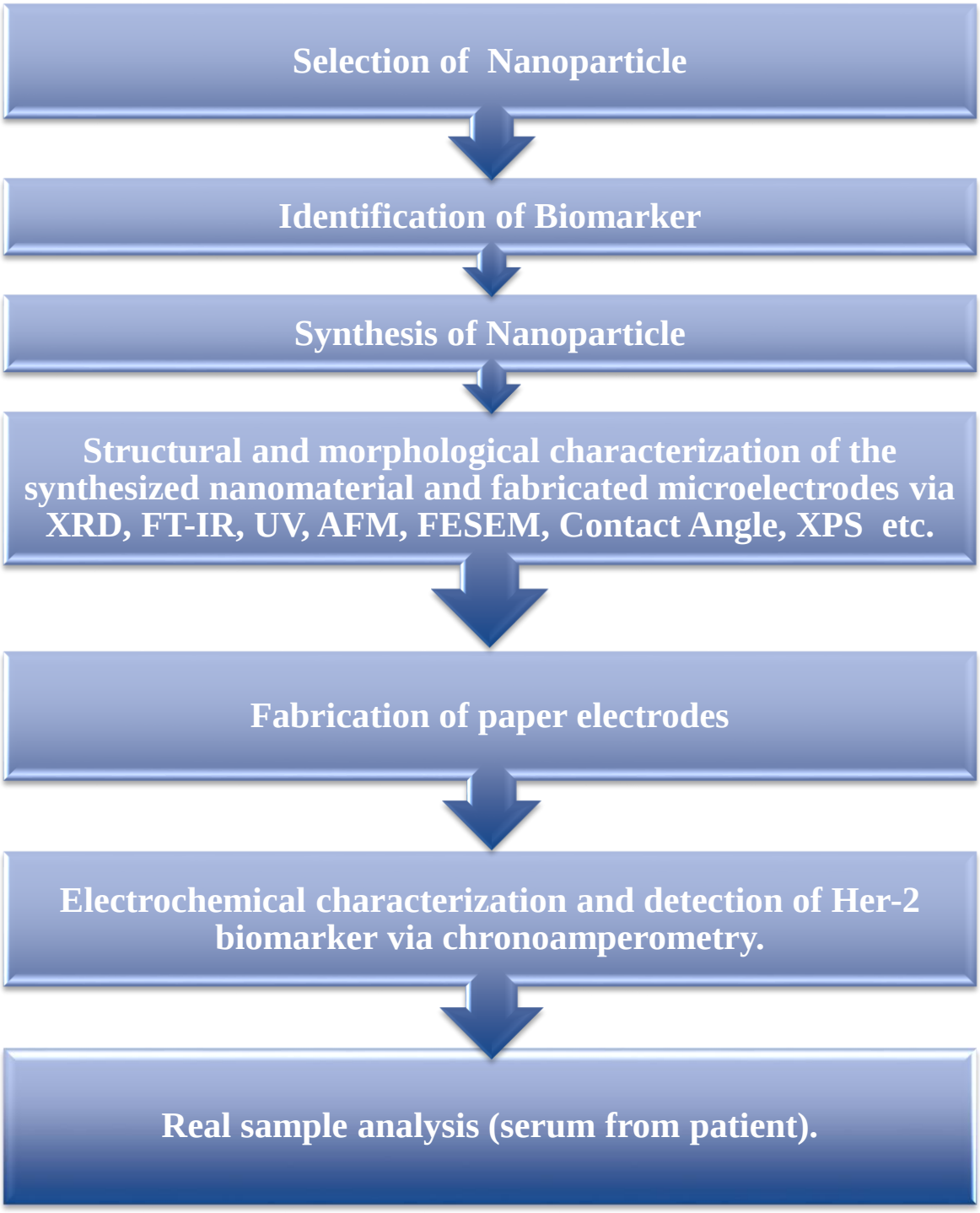

CHAPTER-4

MATERIALS AND METHODS

4.1 Materials

Sodium molybdenum oxide dihydrate ($Na_2MoO_4 \cdot 2H_2O$) and L-cysteine have been purchased from Alfa Aesar and Himedia respectively. Whatman filter paper-1, pore size-11 has been purchased from Merck. The HER-2 antigen biomarker and Anti-HER-2 antibodies are purchased from Sigma Aldrich. Di-sodium hydrogen phosphate dehydrate and sodium dihydrogen phosphate dehydrate are used to wash off the unbound antibodies from the as fabricated MoS_2/Paper composite surface using PBS buffer, purchased from Merck. Milli-Q water (18 M ohm) is been used. All electrochemical studies are carried out at room temperature. All the chemicals used area of analytical grade and used without any further purification.

4.2 Methodology

Hydrothermal method: It is the most widely used method for synthesis of nanoparticles. This method involves high temperature treatment of precursors with water and the synthesis is carried out in a pressurized chamber known as an autoclave It's temperature can be raised above the boiling point of water. The main advantage of using hydrothermal is that it is very simple, scalable and is a readily controlled method as it allows tight control of particle size, its morphology and surface chemistry of the particle by regulating its solution composition and other parameters such as temperature, pH, etc. MoS_2 aggregates on cellulose paper are grown through hydrothermal method and electrochemical characterization and response studies of nanostructured MoS_2 immunoelectrodes have been performed on Electrochemical analyzer.

4.3 Instrumentation &Techniques

The following instruments and techniques have been utilized to conduct experiments that are reported in this work:

4.3.1 XRD (X-Ray Diffraction):

The structural purity and crystallographic properties of the MoS_2/ Paper composite and Bare Whatman filter paper-1 have been analyzed using D/MAX-A Diffractometer Ultima (Rigaku, Japan) with Cu K-α as a source of radiation (λ =1.5406 Å) conducted in between 2θ angles 10-70°. It works on the principle of constructive interference of monochromatic X-Rays on a crystalline sample. Firstly, the cathode ray tube generates X-Rays, which are then filtered and collimated in order to produce monochromatic radiation. This radiation then falls on the sample surface followed by their scattering from the various lattice planes of the sample.The angular distribution of the diffracted x-ray is governed by Bragg's law as:

$$2d\sin\boldsymbol{\theta} = n\lambda \qquad (1)$$

Where, d=interplanar spacing for a crystal lattice, θ=Diffraction angle and λ=Wavelength of electromagnetic radiation. Here, the interaction between the sample and the incident X-rays results in the production of a diffraction pattern, which is then detected along and processed further to generate the final XRD pattern. Thus, this technique is very useful to obtain the crystallite size and crystallographic structure.

Figure 4.1 : X-Ray Diffraction instrument

4.3.2 FTIR (Fourier transform Infrared Spectroscopy):

Fourier transform infrared (FTIR) spectroscopy of MoS_2/Paper Composite have been studied using Thermo-Scientific Nicolet 380 spectrometer in reflectance mode, in the region of 400-4000 cm^{-1}. Fourier transform infrared (FTIR) spectroscopy is a powerful characterization technique for measurement of IR frequency, which is absorbed by the sample when placed in the path of radiation. Because every molecule has its own specific absorption spectrum i.e, IR is mainly used to identify the type of bond between atoms & their functional groups. Its principle is mainly based on the absorption of specific infrared rays, displayed by their molecular bonds depending upon their vibrational intensities. In the FT-IR spectra, presence or absence of certain vibrational frequencies gives valuable information about the structure of a particular molecule. Each functional group has a specific range of vibrational frequencies and is said to be very sensitive to the chemical environment, thus giving valuable information about the presence of functional groups, which are present in the specific sample for their characterization.

Figure 4.2: FTIR Spectrophotometer Instrument

4.3.3 Ultraviolet-Visible Spectrophotometer

In UV Visible spectrophotometer a sample is first exposed to a light wave, which is having energy equivalent to the one released due to the possible electronic transition between the molecules. The given molecule then absorbs a fraction of this light energy and then the electrons in turn are shifted to a higher energy orbital state. Spectrophotometer after that measures the degree of absorption of light energy at different wavelengths and a resulting plot is obtained which known as spectrum in between absorbance (A) and wavelength (λ). Here, we used Perkin Elmer Lambda 950 UV/Visible/NIR spectrophotometer in order to measure the optical density of MoS_2 synthesized. It is based on Beer & Lambert's law, which is given by:

Beer's Law

"It states that there is an exponential decrease in the intensity of the monochromatic light with the increase in the concentration of absorbing substance".

$A = \varepsilon c l$

Where, A is the measured absorbance, ε is the wavelength-dependent molar absorptivity coefficient with units of $M^{-1}cm^{-1}$, c is the analyte concentration and l is the path length.

Figure 4.3: UV/Vis/NIR Spectrophotometer instrument (Perkin Elmer Lambda 950)

Lambert's Law

"When a beam of light is passed through a transparent medium, its intensity is directly proportional to the rate of decrease of intensity with respect to the thickness of medium."

4.3.5 FESEM (Field emission Scanning electron microscope): The surface morphology of the as prepared composite and bare paper has been studied using Field emission scanning electron microscope (FESEM) from Sigma. SmartSEM software is used for operating Carl Zeiss FESEM instrument capable of collecting and generating low vacuum and high-resolution images. It is a very effective and powerful technique that examines object by utilizing a high-energy beam of electrons generated by heated tungsten scanned over a specimen. X-rays and electrons are ejected as soon as the beam hits the specimen, which is then collected by detectors and processed in turn to produce a refined image of the sample in sub-micron levels**.**

Figure: 4.5 Field emission Scanning electron microscope

4.3.6 Contact angle (CA)

It is the angle at which a particular interface (liquid or vapour) meets another solid surface. The contact angle is said to be specific for a given system and is determined by the interaction across the interface. Its value is affected by various parameters such as surface condition, surface roughness, and surface material. Contact angle measures the shape of a liquid droplet resting on a solid surface. A tangent line is drawn from the tip of the droplet to touch the solid surface, the angle obtained between the tangent line and the solid surface is said to be contact angle. Contact angle is a very sensitive technique and can detect various surface properties such as surface energy, wettability and adhesion of a given material. The measurements are carried out to investigate the hydrophilic and hydrophobic behavior of the surface that further correlates with the immobilization of the biomolecule onto the electrodes by a sessile drop method. It is a very useful method to measure the wetting properties of a particular region on a solid surface by measuring the angle between the tangent at the drop boundary and the baseline of the drop. When Contact angle is less than 90°, the surface is known as hydrophilic surface, and if it is more than 90°, it is said to be hydrophobic. If the angle is above ~150°, it is called as super-hydrophobic surface, and if it is less than ~20°, it is said to be super-hydrophilic.

4.3.7 X-ray photoelectron spectroscopy (XPS)

The surface chemical compositions and elemental oxidation states have been determined from the XPS spectra obtained by the PHI 5000 Versa Probe II (ULVAC, PHI Inc.) X-Ray photoelectron spectrophotometer. This spectrophotometer is equipped with a beam (25 W, 15kV) having a 100 microns spot size, produced by a monochromatic Al K-α X-Ray source (1486.6eV). The analyzer is operated in the Constant Analyzer Energy (CAE) mode with a pass energy of 187.85eV for recording the wide survey scan spectra and a pass energy of 58.7eV for recording the subsequent high resolution core level (narrow scan) spectra. The pressure in the analysis chamber is maintained at 1.6×10^{-6} Pa during the entire measurement. The wide survey scan spectra has a measurement energy step size of 0.80eV whereas it is 0.125eV for the narrow scan spectra. The XPS spectrophotometer is connected with a Hewlett-Packard 9836C computer, which is used for collection and storage of XPS data. The instrument

calibration is performed considering all the procedures suggested by the manufacturer and is calibrated considering peak position of C1s at 284.5eV.

4.3.8 Electrochemical system

All the Electrochemical studies have been performed on Autolab Galvanostat/ Potentiostat (Metrohm, Netherlands). MoS2 paper is used as the working electrode, platinum (Pt) as the counter electrode, and silver-silver chloride (Ag/AgCl) as the reference electrode using three-electrode system. PBS (Phosphate buffer solution) solution (50 mM at pH 7) 5 mM $[Fe(CN)_6]^{3-/4-}$ has been used as the redox species in the form of electrolyte in the frequency range of 100KHz to 10Hz.

Figure: 4.6 Autolab Galvanostat/Potentiostat Instrument (Metrohm, The Netherlands)

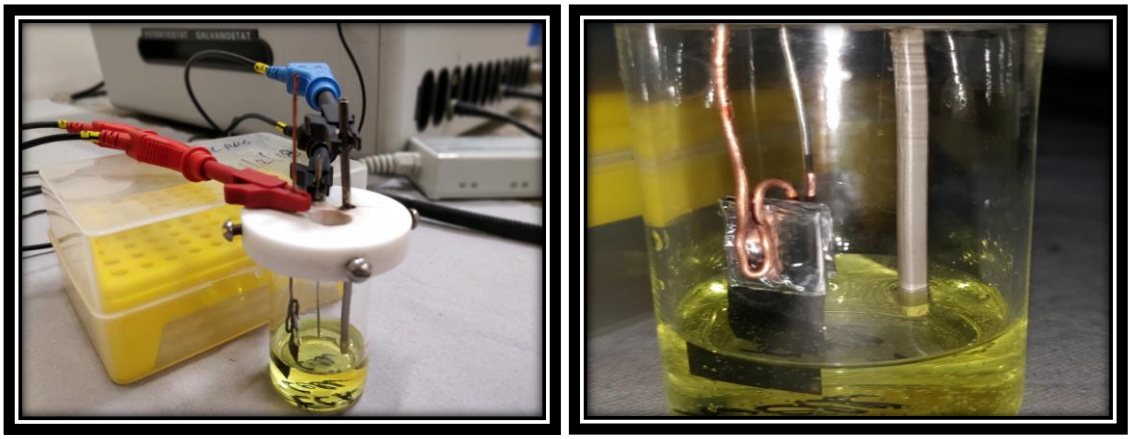

Figure: 4.7 A three-electrode system

CHAPTER-5

EXPERIMENTAL SECTION

5.1 Synthesis of MoS_2 on cellulose paper

One step, hydrothermal method has been used for the synthesis of the MoS_2-Cellulose which involves two steps namely seed coating process followed by hydrothermal. Briefly, 36.29 mg of sodium molybdate dehydrate (10mM) taken and homogenously dispersed in 15 ml of double distilled water by magnetic stirrer for 1 h. Similarly; 36.34 mg of L-cysteine (20mM) is separately dispersed in 15 ml double distilled water.

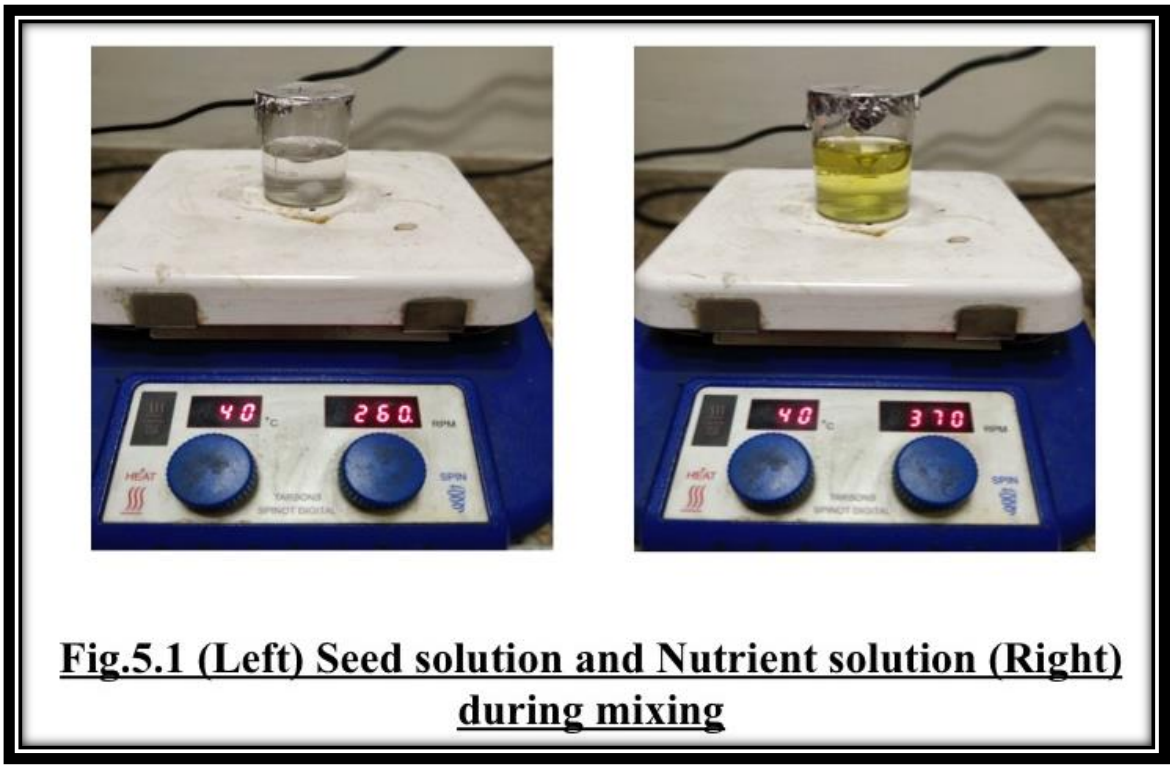

Fig.5.1 (Left) Seed solution and Nutrient solution (Right) during mixing

After that, both the solution was mixed and the reaction mixture was kept on magnetic stirrer for 1 hour. Named this solution as "**SEED SOLUTION".**

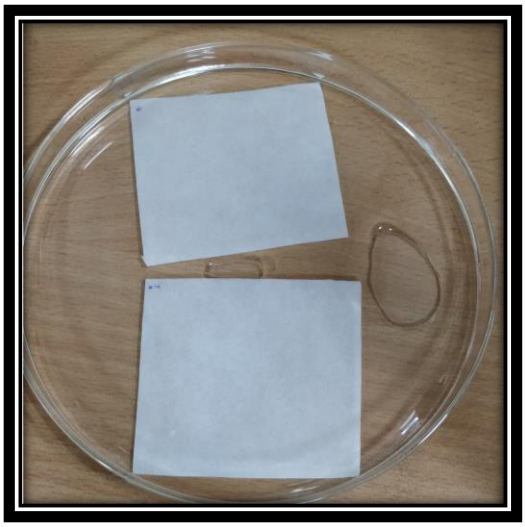

Figure: 5.2 Whatman filter paper dipped in seed solution

Whatman filter paper no.-1(pore size 11µm) was used as cellulose substrate for growth of MoS_2 nanoparticles. A standard cellulose paper size of 5*6 cm was taken for optimizing the reaction conditions everytime. The paper substrate was dipped in seed solution for 1 hour followed by drying at 80°C for 30 minutes in hot air oven.

The "**NUTRIENT SOLUTION"** was prepared by mixing 362.925 mg sodium molybdate dehydrate (50mM) and 363.46 mg L-cysteine (100mM) in 30ml DI water each. The seed coated cellulose paper and nutrient solution were then transferred to Teflon line autoclave and was kept at 180°C for 20 hours. The autoclave was allowed to naturally cool down.

Figure: 5.3 Whatman filter paper after hydrothermal reaction

The deposited MoS_2 cellulose paper was then washed with deionized water 2-3 times and was then dried at 70°C for 15 minutes to obtain the final product. A black-greyish-colored paper was obtained and further studies were done.

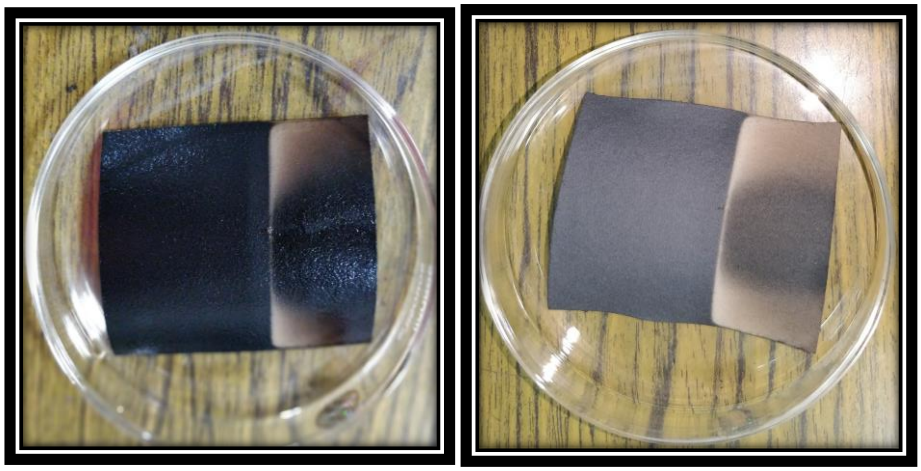

Figure: 5.4 (Left) MoS_2 paper after washing with deionized water and (Right) after drying

5.2 Fabrication of the BSA/Anti-HER-2/MoS_2 paper electrode

A solution of HER-2 antibody (50 μg mL^{-1}) was prepared in PBS (pH 7). 30 μL of this antibody solution was taken and the resulting reaction mixture was incubated at room temperature for 20 min, and subsequently drops casted on to the 1*2.5 cm MoS_2 paper composite electrode in a uniform manner. Lastly, 30 μL of BSA (0.1 mg mL^{-1}) was used to block the non-specific sites on the electrode. Thus, BSA/Anti-HER-2/MoS_2 paper composite immunoelectrode was fabricated and was stored at 4℃ when not in use.

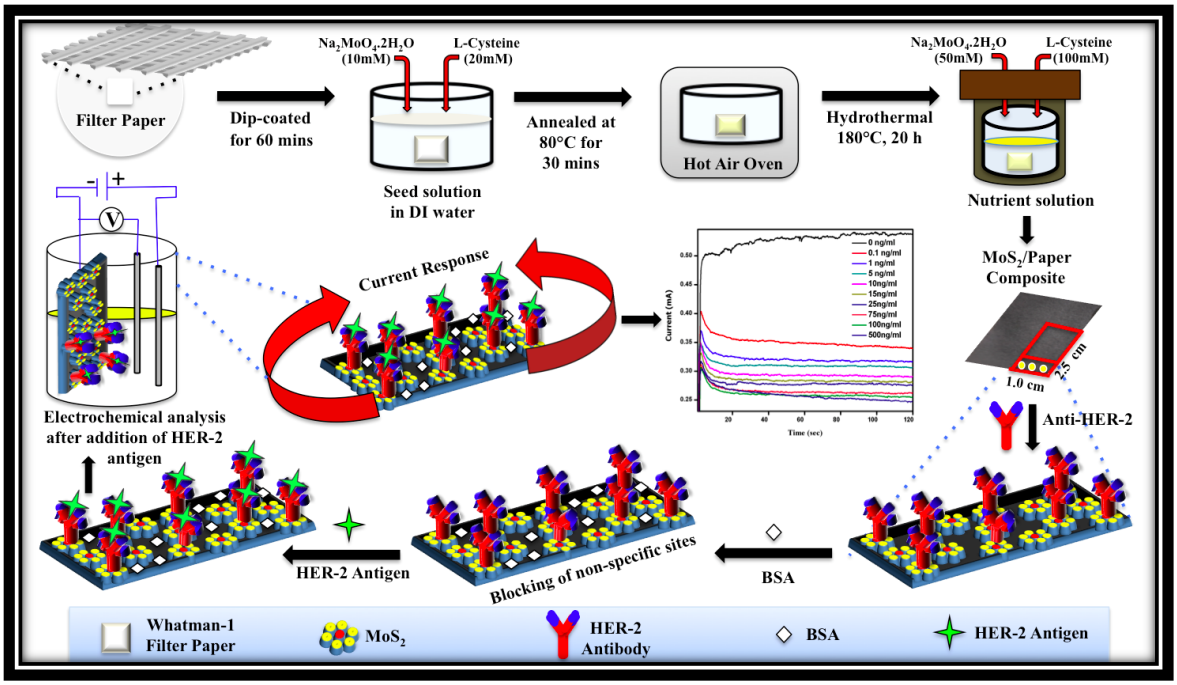

Fig. 5.5 Schematic depicting the steps involved in the synthesis of MoS_2 /Paper composite, followed by fabrication of BSA/Anti-HER-2/MoS_2 /Paper composite immunoelectrode

CHAPTER-6
RESULTS AND DISCUSSIONS

6.1 Structural and morphological characterization

6.1.1 X-Ray Diffraction (XRD)

The structural purity and the crystallographic properties of the MoS_2/Paper composite and Bare Whatman-1 filter paper have been analyzed using their X-ray Diffraction Spectra. The purity and crystallinity of the nanomaterial's structure has a decisive impact on the electrical, mechanical and crystallographic attributes of the synthesized composite. The sharp diffraction peaks of the MoS_2/Paper composite displays its partially crystalline structure. The peaks observed at 16.45° and 22.68° are attributed to cellulose paper corresponding to (110) and (200) planes respectively. [29] Also, the presence of cellulose peaks within the MoS_2/Paper composite depicts the ability of cellulose paper to withstand high temperature under hydrothermal conditions without undergoing any degradation. Fig. 6.1.1 Shows the comparison between the XRD pattern of bare paper and MoS_2 grown on cellulose paper. The diffraction peaks occurring at 14.78°, 34.10° and 46.74° are ascribed to the (002), (012) and (103) planes of MoS_2 respectively, which confirms the growth of pristine MoS_2 over the cellulosic network. [32] The maximum intensity diffraction peak is obtained from the (200) plane of the composite signifying the favored direction of MoS_2 crystal growth along this plane. Here, it is observed that the favored growth direction of MoS_2 has changed during its synthesis on the cellulose substrate. A decrease in diffraction angles has been observed in all the peaks corresponding to the MoS_2/Paper composite when compared with that of bare Whatman-1 filter paper. This confirms the homogeneous nucleation of MoS_2 on the surface of cellulose paper. However, due to the low synthesis temperature (180°C), broadening in all the MoS_2 peaks is observed which correlates with the lower crystallinity of the synthesized nanostructure. [30] Although cellulose is suppressing the diffraction peaks of pristine MoS_2 by preserving its inherent crystal structure, still a considerable increase in the intensity of its peaks can be observed, with their shapes remaining unchanged even after hydrothermal synthesis. This is suggestive of an improved crystallinity of the composite in comparison with the bare paper. However, the lower intensity peaks (2θ=14.78° and 16.45°) corresponds to the amorphous portion of the synthesized composite with larger interplanar spacings, whereas the higher intensity peaks (2θ=22.68, 34.10° and 46.74°) are attributed to the crystalline portion of the composite with lower interplanar spacing between successive lattice fringes. Successively, the interplanar distances have been calculated for all the above peaks and

are found to be 0.598nm, 0.538nm, 0.3914nm, 0.263nm and 0.1951nm respectively, derived from the Bragg's law which is given by the equation:

$$n\lambda = 2\, d_{(hkl)}\, \mathrm{Sin}\theta \qquad (2)$$

Here, λ=Wavelength of the source (0.15406 nm), n= Order of diffraction peaks (Here n=1), θ= Diffraction angle of the corresponding lattice plane.

Further, the average crystallite sizes corresponding to the highest intensity diffraction peak were calculated for the bare Whatman-1 filter paper and MoS_2/Paper composite using the Debye- Scherrer equation:

$$D(hkl) = \frac{k\lambda}{\beta\, \mathrm{Cos}\theta} \qquad (3)$$

Where, $D_{(hkl)}$= Crystallite size perpendicular to the (hkl) plane, $\beta_{(hkl)}$= Full width at half maximum of the diffraction peak corresponding to the (hkl) plane. Also, k= Scherrer Constant (0.9), $\theta_{(hkl)}$ = Bragg's diffraction angle corresponding to the (hkl) plane and λ= Wavelength of Cu-Kα line. Hence, the crystallite sizes of bare Whatman-1 filter paper and the MoS_2/paper composite are found to be 6.465nm and 6.991nm respectively. The larger crystallite size of the MoS_2/Paper composite than bare filter paper suggests that the larger the crystallite size, the higher is the intensity of the diffracted signal. [31]

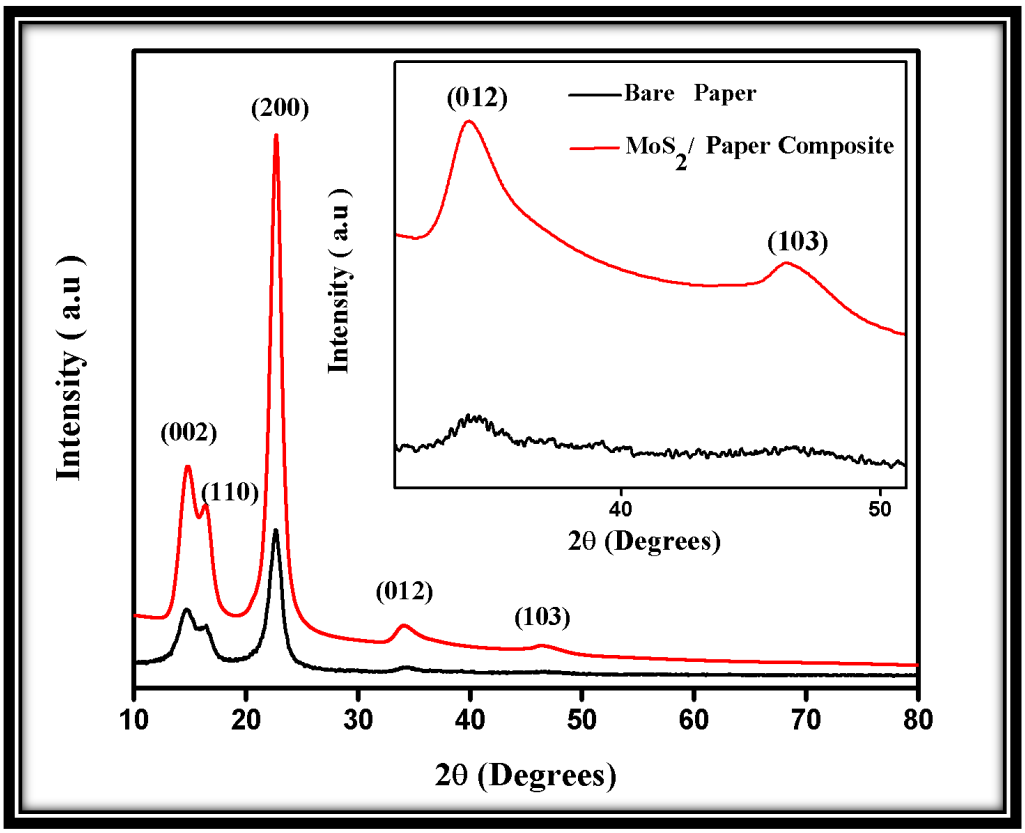

Figure 6.1.1: XRD Spectra: Bare Whatman-1 Filter Paper (Black) , MoS_2/ Paper Composite (Red)

6.1.2 Fourier Transform Infrared Spectroscopy (FTIR):

The chemical compositions of Bare Whatman-1 Filter Paper, MoS_2/Paper Composite and Anti-HER-2/ MoS_2/ Paper Composite have been investigated using Fourier transform Infrared Spectroscopy FTIR (ATR) as shown in Fig.6.2 (a), (b) and (c). FTIR spectrum of Bare Whatman-1 Filter Paper exhibits peak at 3334, 1654, 1314, 1160, 1053, 897cm $^{-1}$ attributed to Hydrogen bonded OH stretching in a cellulose chain [62], OH bending vibrations of absorbed H_2O molecules [63], CH_2 wagging at the C_6 position of the cellulose, C-O-C stretching at β-1,4 glycosidic linkages[64], C-C, C-OH, C-H ring and side group vibrations, C-O-C, C(C-O) and C-CH D-formation and assymetric stretching[64].

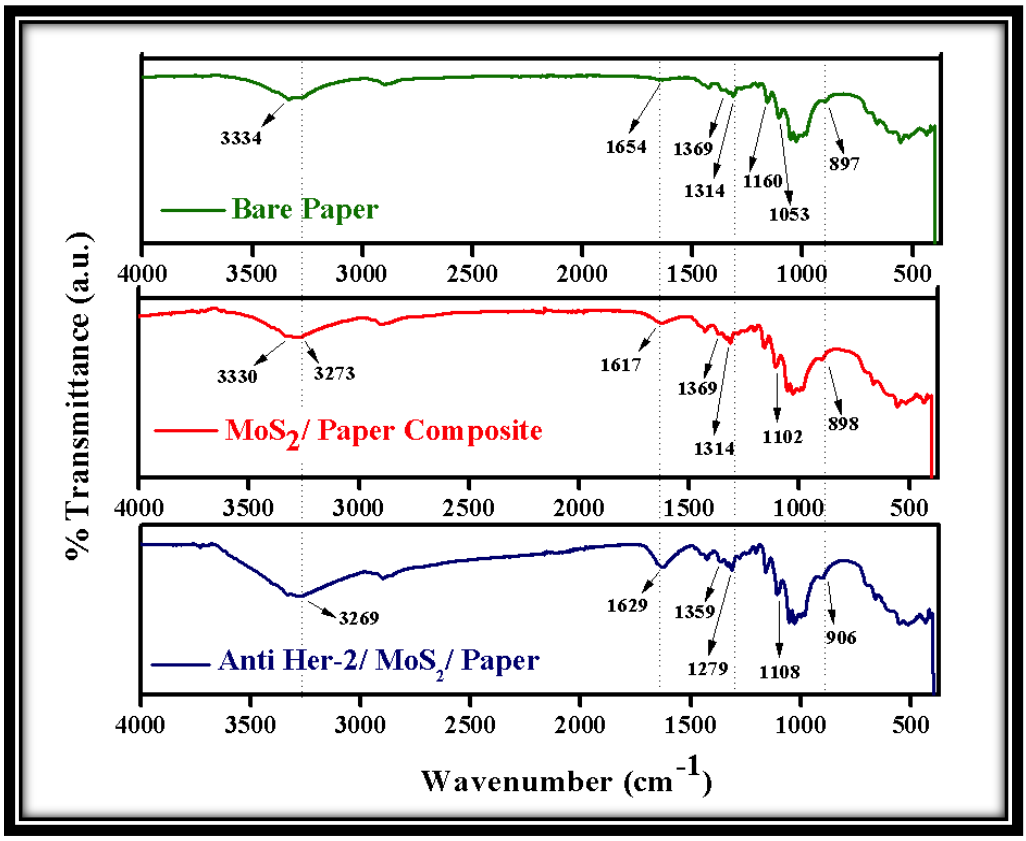

Figure 6.2: FTIR (ATR) Spectra – (a) Bare Whatman-1 Filter Paper (b) MoS_2/Paper Composite (c) Anti-HER-2/ MoS_2/ Paper Composite

In contrast, MoS_2/Paper Composite exhibits a Red shift in the Hydrogen bonded OH stretching peak to 3330cm^{-1}[62]. A new peak also emerges at 3273 cm^{-1} corresponds to OH stretching in carboxylic group of l-cysteine. Further a band at 1617 cm^{-1} is attributed to NH_2 Scissoring mode, which is suggestive of the presence of l-cysteine in MoS_2. The increase in intensity of the band at 1314 cm^{-1} as compared to that of bare paper is attributed to C(O)-O vibrations.[64] The peak at 1102 cm^{-1} exhibits a significant shift from that of bare paper and is attributed to Mo-O stretching vibrations. Lastly the peak at 898 cm^{-1} exhibits an increase in intensity and is attributed to S-S vibration in MoS_2. [64]

Upon antibody immobilization the FTIR spectra of Anti-HER-2/ MoS_2/ Paper Composite exhibits a Red shift in the O-H stretching vibration in carboxylic group of Anti-HER-2 at 3269 cm^{-1} [62]. Further a peak at 1629 cm^{-1} exhibits a blue shift and a significant increase in its intensity as compared to MoS_2/Paper Composite. This change is attributed to the primary amine group of Anti-HER-2. The band at 1279cm^{-1} exhibits a red shift in the band in comparison to MoS_2/ Paper Composite and is attributed to C(O)-O stretching vibrations at the carboxylic sites of Anti-HER-2. Further, the Mo-O stretching vibration at 1108cm^{-1} exhibits a blue shift due to interaction of Anti-HER-2. Finally, the band at 906 cm^{-1} also exhibits the blue shift in comparison with that of MoS_2 and is attributed to the interaction of S-S bond with Anti-HER-2. [64]

6.1.3 UV-Visible Spectroscopy Studies

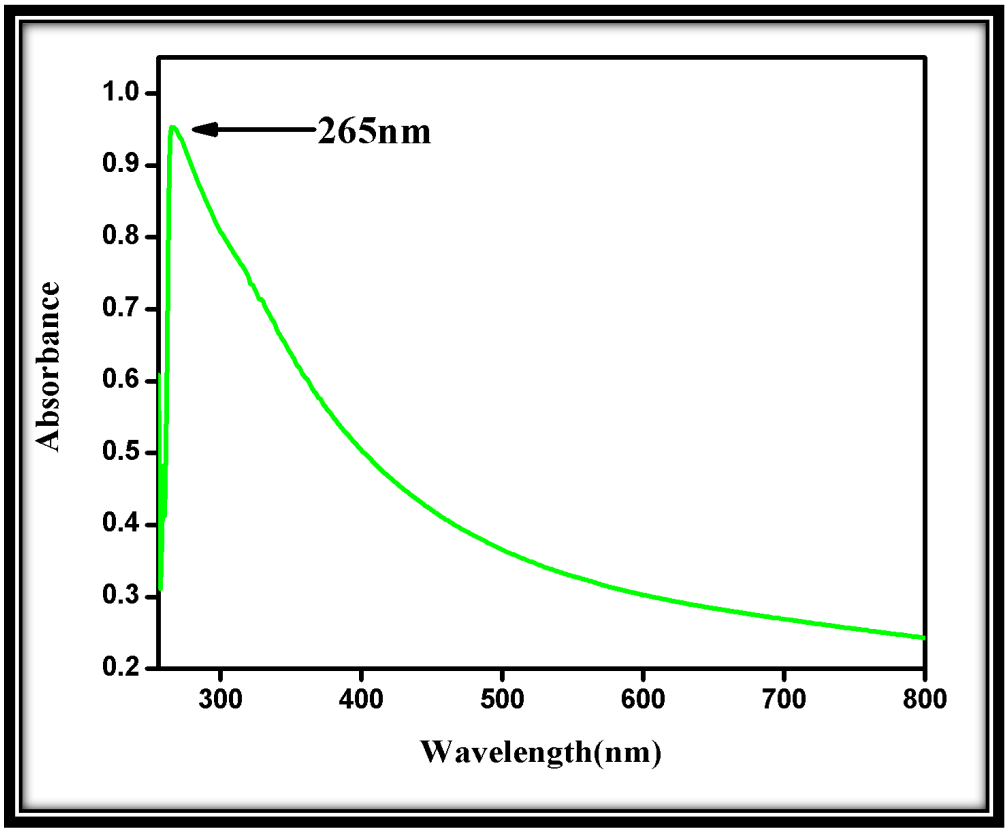

Figure: 6.3 UV-visible-NIR spectrum of MoS_2 aggregates

Optical absorption spectrum has been measured using ultraviolet–visible–near-infrared (UV–Vis–NIR) spectroscopy (path length = 1 cm) in order to understand the absorption characterstics. MoS_2 nanoflowers were dispersed in DMF (Dimethylformamide) and were sonicated for 12 hours. The UV-Vis optical absorption spectra have been recorded in the wavelength range of 250–750 nm, at room temperature as shown in Fig.6.3. After sonicating it for few seconds, spectra was immediately recorded to ensure complete redispersion of the aggregates of MoS_2. A strong absorption peak is observed at 265nm showing the absorption spectra of MoS_2 cellulose composite.

6.1.4 Atomic Force Microscopy (AFM)

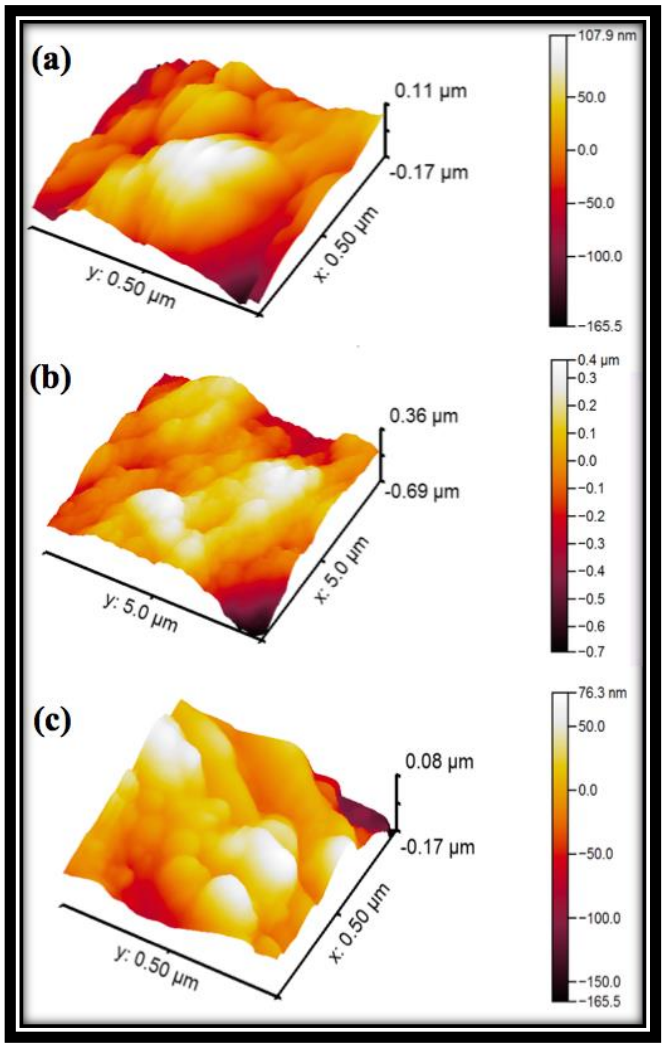

Figure 6.4 : AFM images - a) Bare Whatman-1 Filter Paper
(b) MoS_2/Paper Composite (c) Anti-HER-2/ MoS_2/ Paper Composite

AFM of Bare Paper, MoS_2/ Paper Composite and Anti-HER-2/ MoS_2/ Paper Composite electrode have been performed to study the respective surface morphology as shown in Fig 6.4. (a-c). From Fig (a), Bare paper displays a smooth surface with an rms roughness of ~42.07nm. It suggests that Whatman-1 filter paper has a uniform surface. Further, the growth of MoS_2 nanocoating on paper, led to a large increase in the rms roughness to ~150.1nm. The significant increase in roughness is attributed to high specific surface area of the nanostructure, leading to the exposure of its active sites. Lastly, the physisorption of Anti-HER-2 on the MoS_2/ Paper Composite resulted in a drastic decrease in the rms roughness to ~34.45nm. This decrease in surface roughness may be attributed to the globular structure of the antibody, which blocks the active sites of the MoS_2 nanocoating.

6.1.5 Field Emission Scanning Electron Microscopy (FESEM)

FESEM analysis has been performed to study the morphology of MoS_2 grown on cellulose substrate. MoS_2 growth can be clearly seen on the microporous structure of cellulose fibers representing the capability of cellulose paper to withstand high temperature. It has been obtained that 180°-200°C temperature is suitable for the growth of MoS_2, whereas cellulose paper is found to degrade around 275 °C. FESEM analysis is been performed to study the morphology of bare paper, MoS_2/Paper and Anti-HER-2/ MoS_2/Paper Composite at low and high magnifications. Fig 6.5 (a) and (b) shows low and high magnification images of cellulose fibers. Self- assembly of MoS_2 nanoparticles can be clearly seen in the form of micro-flower like morphology as shown in fig. 6.5(c) and (d). Further FESEM of HER-2 immobilized on MoS_2/Paper Composite can be seen as shown in fig 6.5(e) and (f) clearly depicting the binding of antibodies over the sub-micron flower like morphology of MoS_2 aggregated particles grown on the cellulose substrate. These self-assembled MoS_2 nanostructures are large and rounded with antibodies agglomerating around them.

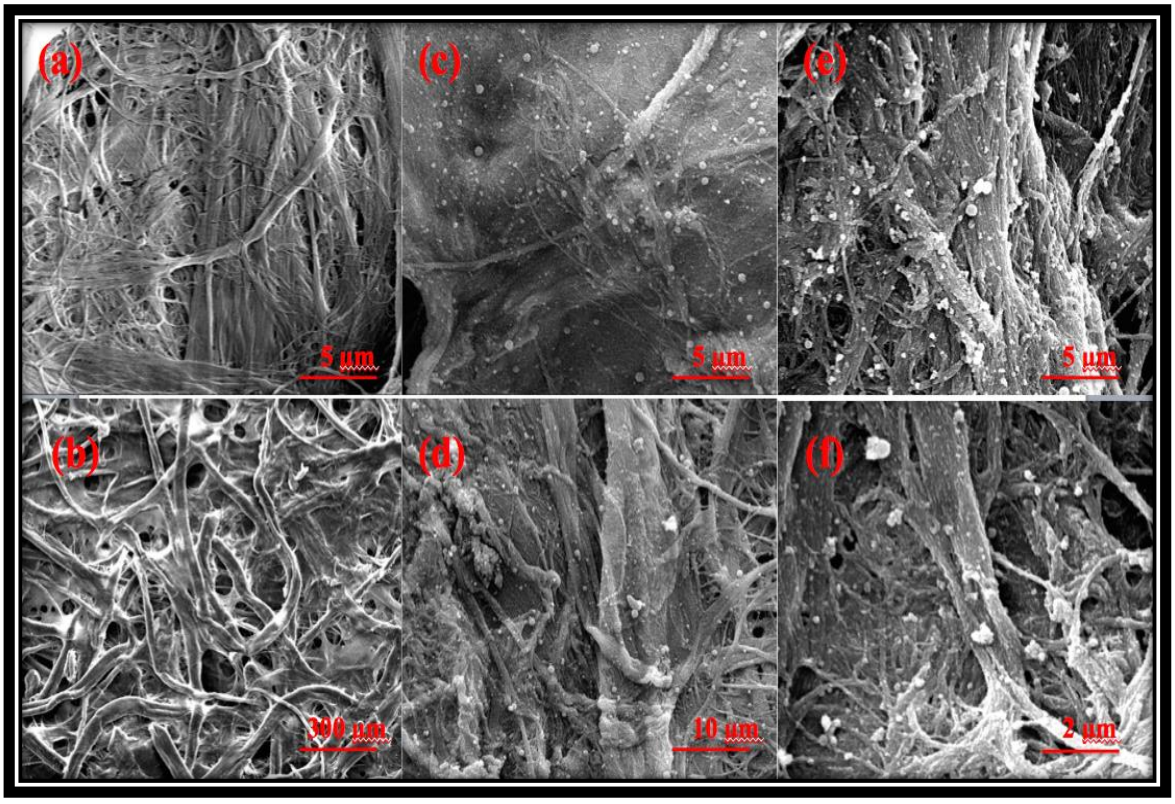

Figure 6.5: SEM images- Bare paper (a-b), MoS_2 /Paper Composite(c-d), Anti-MoS_2 / Paper Composite(e-f)

6.1.6 Contact Angle Studies

The surface wettability of Bare Whatman filter paper-1, MoS_2/Paper and Anti-HER-2/MoS_2/Paper Composite have been measured using Contact angle. The strong attraction of hydroxyl groups present in the cellulose fibers with water and fluid through capillary action quickly absorbs water and makes it hydrophilic in nature. It is said that surface roughness at times amplifies the wettable properties of materials, which makes a hydrophobic surface more hydrophobic (Wenzel et al.) Therefore, the contact angle (CA) value of the Bare Whatman filter paper-1 is found to be approaching to zero as shown in Fig. 6.6 (a). Further, it has been found that covering the channel of fibers controls the wicking behavior of Bare Whatman filter paper-1 and this is achieved by hydrothermal growth of MoS_2 on its surface. Thus, the seed and nutrient growth of MoS_2 precursors led to an increase in the hydrophobicity of paper increasing its contact angle to 110^0 as shown in Fig.6.6 (b). The MoS_2 /Paper is then immobilized by HER-2 antibody. The presence of amine (-NH_2) group and the carboxylic group (-COOH) in the antibody lead to a decrease in its contact angle to 100° as shown in Fig.6.6 (c) depicting the hydrophilic nature of NH_2 group present in HER-2 antibody.

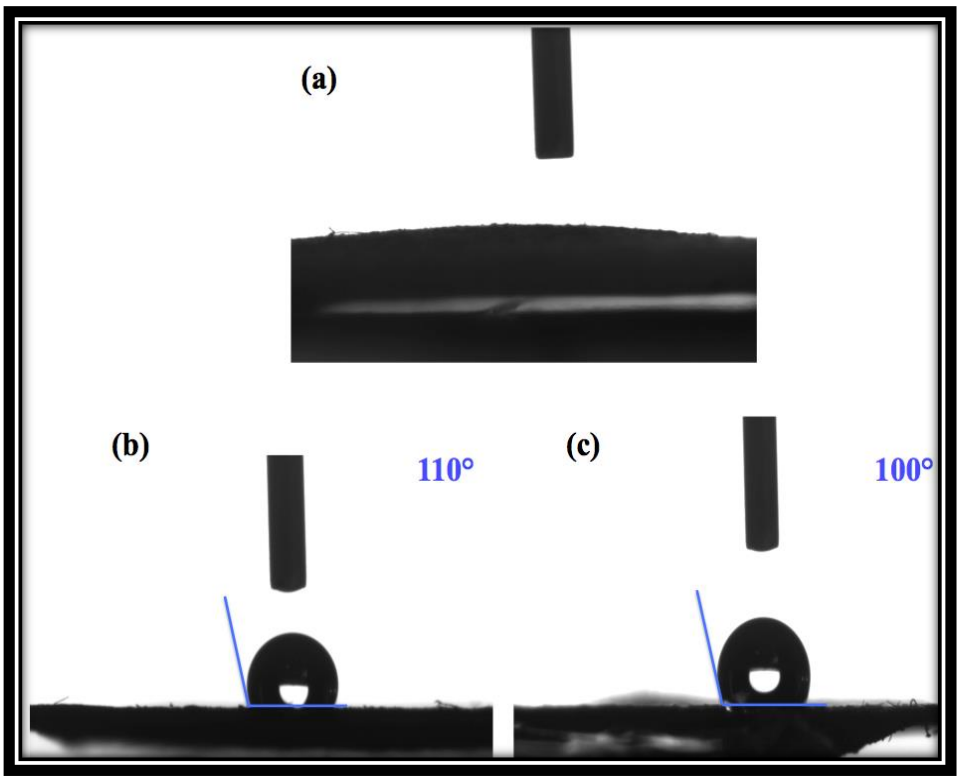

Figure 6.6: Contact angle images - (a) Bare paper (b) MoS_2 / Paper Composite (c) Anti-MoS_2 / Paper Composite

6.1.7 X-ray photoelectron spectroscopy (XPS)

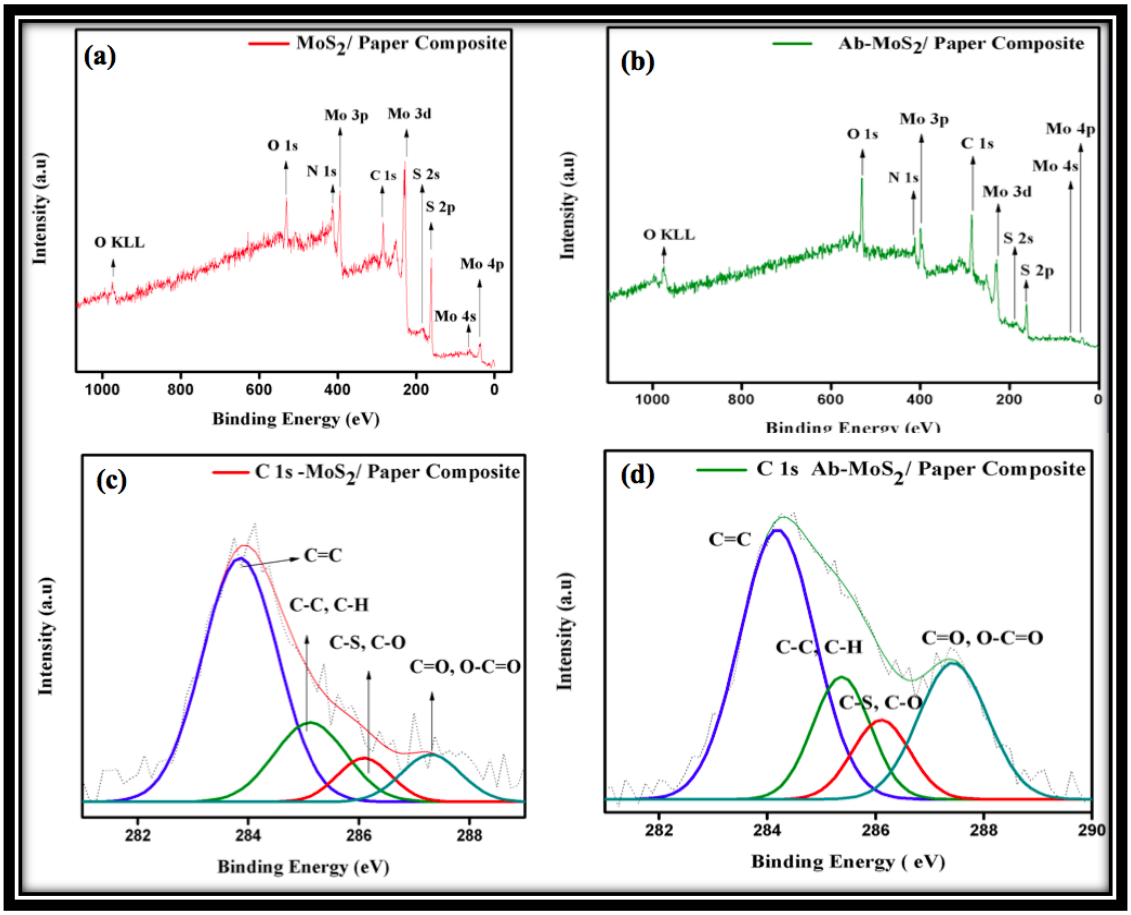

Figure 6.7: XPS Investigations of MoS_2 / Paper Composite (LEFT) & Anti-HER-2/ MoS_2 / Paper Composite (RIGHT)

(a) and (b) Wide scan survey spectrum

(c) and (d) C 1s core level spectrum

The wide survey scans and high resolutions scans of the MoS_2/Paper composite and the anti-HER-2/MoS_2/Paper composite have been obtained using X-ray photoelectron spectroscopy (XPS). The C1s core level spectra can be deconvoluted into four peaks- 283.85, 285.121, 286.09 and 287.30eV attributed to sp^2 Carbon [41], sp^3 Carbon & C-H bond [42], C-S bond[43] & C-O bond [44], C=O[44] & O-C=O [41], respectively. Whereas, upon antibody immobilization, these peaks shift towards the higher binding energies- 284.18, 285.37, 286.10 and 287.43eV respectively. Additionally, an increase in the contribution of the peaks] after antibody immobilization suggests the presence of anti-HER-2 carboxylic moieties (HO-C=O).

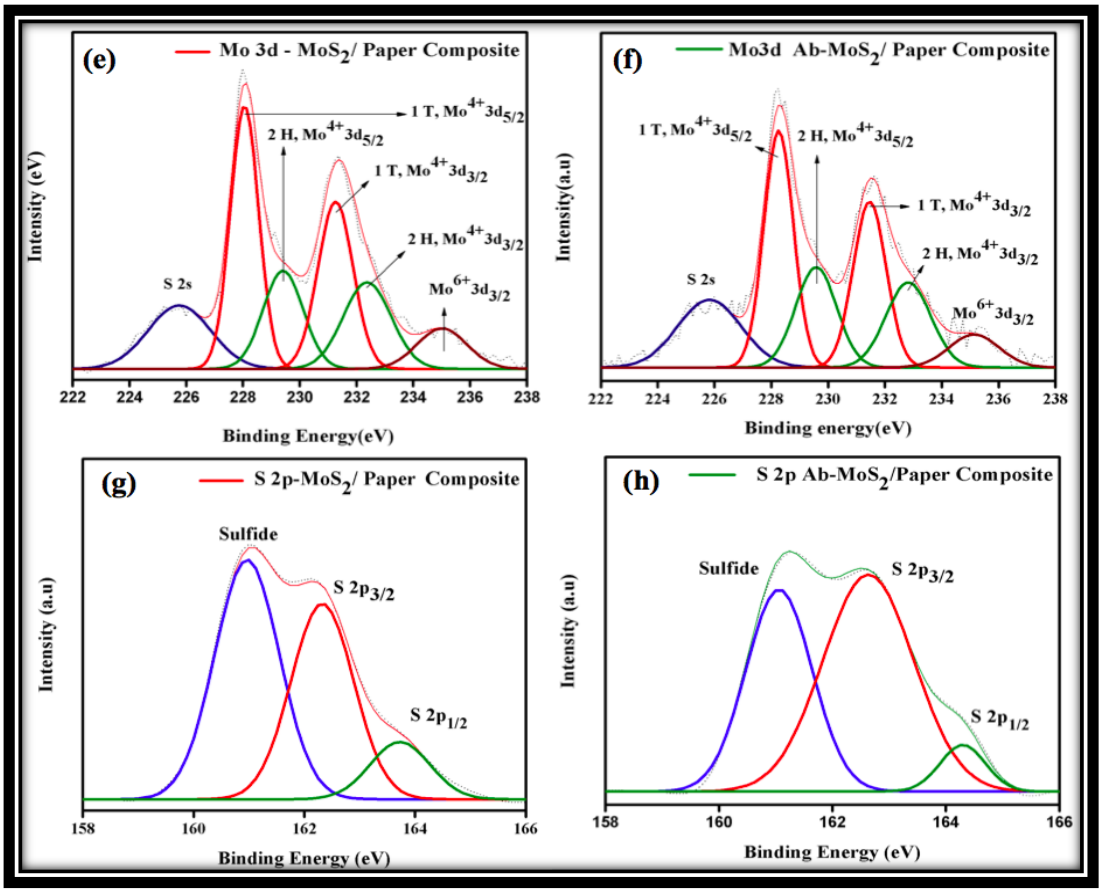

Figure 6.8: XPS Investigations of MoS_2 / Paper Composite (LEFT) & Anti-HER-2/ MoS_2 / Paper Composite (RIGHT)

(e) and (f) Mo3d core level spectrum

(g) and (h) S2p core level spectrum

In the case of Mo3d, a characteristic doublet was obtained at 229.1 and 232.37 eV as Mo $3d_{5/2}$ and Mo $3d_{3/2}$, confirming the formation of the + 4 oxidation state of Mo in the 2-H phase of the MoS_2 aggregates.[48] These peaks shifted to 229.57 eV and 232.82eV after antibody immobilization. Additionally, another doublet of Mo3d can be observed at 228.05 eV and 231.26 eV attributed to Mo $3d_{5/2}$ (+4) and Mo $3d_{3/2}$ (+4) respectively in the 1-T phase of MoS_2 with a shift to 228.25 and 231.46eV respectively in the anti-HER-2/composite paper.[47] A weak peak corresponding to S2s was obtained at 225.76 eV in the MoS_2-paper composite, whereas in anti-HER-2/composite paper it was observed at 225.82 eV.[46] Another feeble peak was obtained at 235.01eV and 235.13eV respectively in MoS_2-paper composite and anti-HER-2/composite paper

corresponding to Mo $3d_{3/2}$ (+6 oxidation state), which signifies the presence of MoO_3 species due to surface oxidation of MoS_2 under air exposure.[48]

Similarly, S2p core level spectra are deconvoluted into three peaks at 160.97, 162.32 and 163.73 respectively in MoS_2-paper composite which are attributed to the di-sulfide[59], $Sp_{3/2}$[60] and $Sp_{1/2}$[61] peaks respectively whereas in anti-HER-2/composite paper, the peaks were shifted to higher binding energies i.e, 161.06, 162.63 and 164.3 eV respectively.

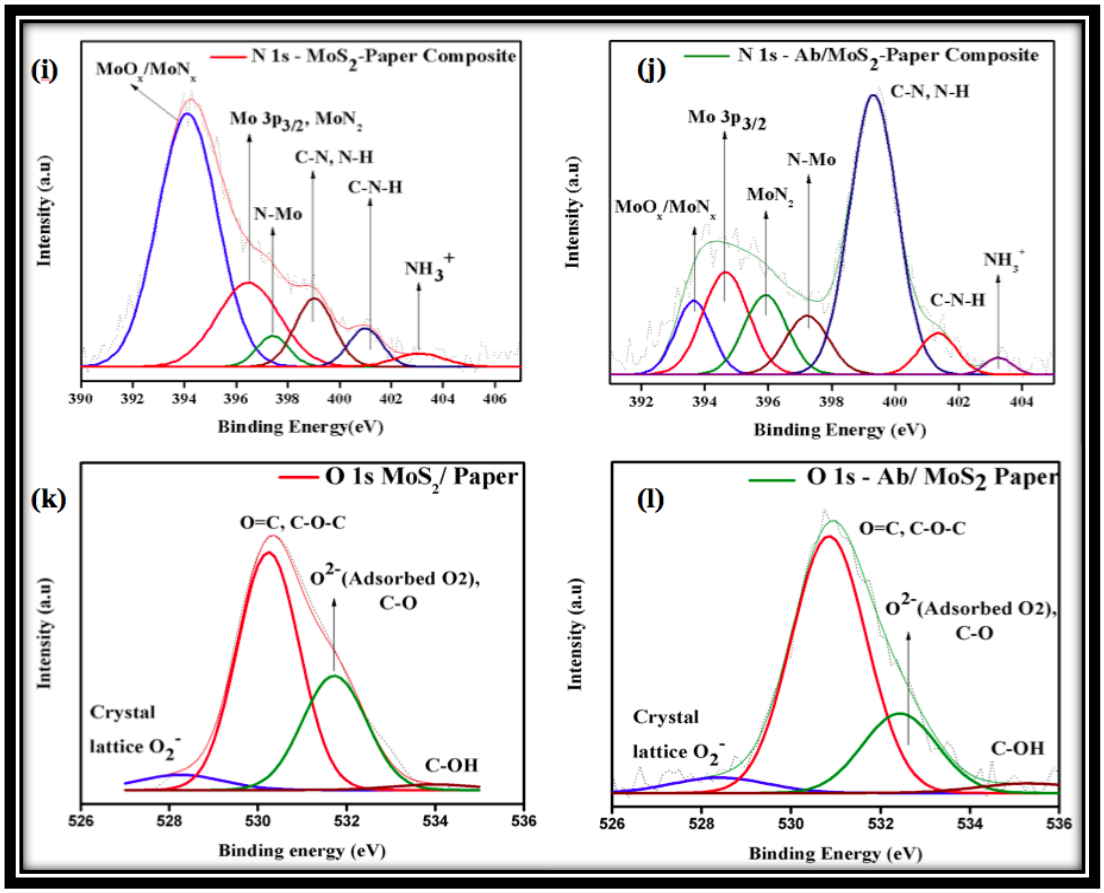

Figure 6.9: XPS Investigations of MoS_2 / Paper Composite (LEFT) & Ant i-HER-2/ MoS_2 / Paper Composite (RIGHT)

(i) and (j) N1s core level spectrum

(k) and (l) O1s core level spectrum

In O1s, four deconvoluted peaks are obtained at 528.25, 530.24, 531.72 and 534 eV respectively. The highest binding energy peak at 534 eV is attributed to the C-OH bonds, possibly arising from l-cysteine residues incorporated in the MoS_2-paper composite during synthesis.[58] The next peak at 531.72 eV corresponds to the chemisorbed oxygen on the MoS_2 surface.[57] The next peak at 530.24 eV corresponds to the O=C, C-O-C bonds, possibly arising from l-cysteine residues in the MoS_2-paper composite (O=C) along with exposed regions of the cellulose backbone (C-O-C).[56] The last peak at 528.25 eV arises from the MoS_2 crytal lattice defects (lattice oxygen). [55]These peaks exhibited a shift to higher binding energies in the anti-her2/composite paper and were obtained at 528.42, 530.85, 532.43 and 535.33eV respectively which is a result of the presence of the carboxylic (HO-C=O) moieties of anti-HER-2.

Lastly, in the N1s core level spectra, the deconvoluted peaks are obtained at 394.12, 396.48, 397.42, 399.03, 400.99 and 403.09 eV respectively for the MoS_2-paper composite. The first three peaks can be attributed to the presence of MoO_x/MoN_x bonding (394.12 eV) [49], Mo $3p_{3/2}$ (+6) & MoN_2 (396.48 eV) [50] and N-Mo (397.42 eV) [51] as the defects introduced in the MoS_2 nanostructure during the hydrothermal reaction of the precursors l-cysteine (amino acid) and ammonium molybdate tetrahydrate. The remaining three peaks can be attributed to the C-N & N-H bonding (399.03 eV)[52], C-N-H amino group bonding (400.99 eV) [53] and NH_3^+ from the protonated primary amines (403.09 eV).[54] These three peaks are possibly arising from the nitrogen-rich l-cysteine residues incorporated in the MoS_2-paper composite post synthesis. Similarly, the deconvoluted peaks for the anti-HER-2/composite paper are obtained at 393.64, 394.65, 395.92, 397.26, 399.32, 401.35 and 403.25 eV respectively. A reduction in the intensity of the peak at 393.64 eV suggests that the layer of antibodies over the MoS_2 coating suppresses the contribution due to MoOx/MoNx. A splitting in the combined peak obtained earlier at 396.48 eV for the MoS_2-paper composite, into two peaks at 394.65 and 395.92 eV for the anti-HER-2/composite paper signifies the individual contributions from Mo $3p_{3/2}$ (+6) and MoN_2 respectively. Finally, the drastic increase in the peak intensity at 399.32 eV corresponds to the enhanced contributions of the C-N and N-H bonding after the immobilization of amine-rich anti-HER-2.

Table 2.4: XPS Elemental Identification and Quantification Data

Elemental Orbital	Peak Binding Energy (eV)		FWHM (eV)		Atomic %	
	MoS_2/ Paper Composite	**Anti-HER-2/MoS_2/ Paper Composite**	**MoS_2/ Paper Composite**	**Anti-HER-2/MoS_2/ Paper Composite**	**MoS_2/ Paper Composite**	**Anti-HER-2/ MoS_2/ Paper Composite**
Mo3d	**235.01**	**235.13**	**2.069**	**2.069**	**12.9**	**4.6**
N 1s	**394.12**	**403.26**	**2.70**	**0.974**	**24.8**	**17**
C 1s	**287.30**	**287.43**	**1.26**	**1.50**	**29.1**	**49.7**
O 1s	**530.24**	**535.33**	**1.63**	**2.72**	**12.3**	**19.5**
S 2p	**160.96**	**164.29**	**1.37**	**0.94**	**21.0**	**9.2**

6.2 Electrochemical characterization

6.2.1 Optimization results of MoS_2/Paper composite

Different concentration of MoS_2 paper has been optimized before standardizing the final concentration. In case of medium concentration, we took 10mM sodium molybdate dehydrate and 20 mM L-cysteine for seed solution and for nutrient solution 50mM and 100mM of sodium molybdate dehydrate and l-cysteine was used. Similarly for high and half concentration exactly twice and half of these concentrations is used for synthesizing MoS_2 paper keeping the ratio same in all the cases. It is found that the current greatly reduced in case of half concentration followed by medium concentration paper. The reduction in half concentration MoS_2 paper current is probably due to the incomplete growth of precursor molecules, as the seeding process couldn't be completed, resulting in decrease in the overall current. Whereas, current reduced in case of high concentration because of agglomeration of MoS_2 nanoparticles on the surface of cellulose paper resulting in the stacking onto the surface thereby, increasing the overall resistance thus, reducing the current.

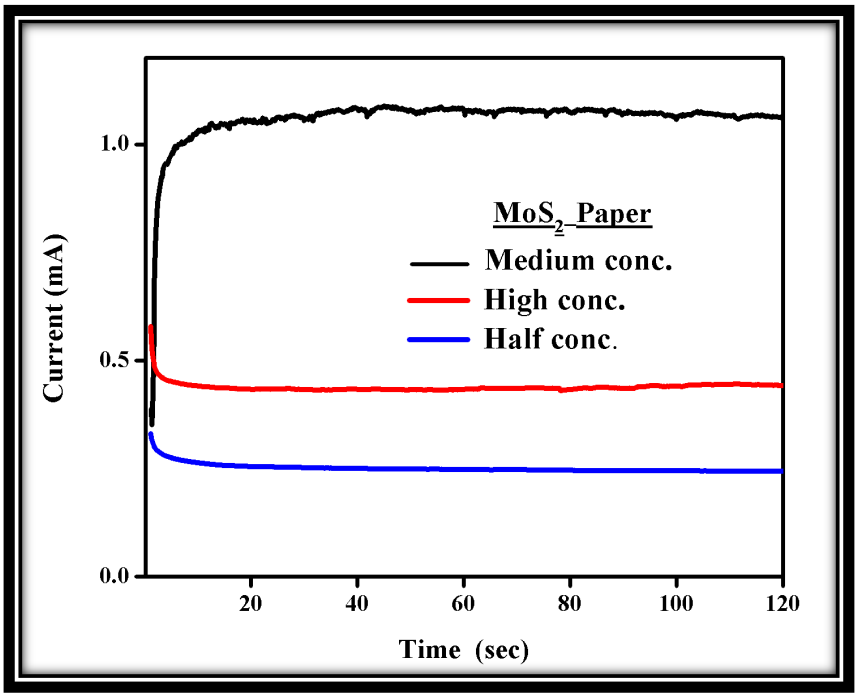

Figure 6.10 Chronoamperometry results comparing different concentrations of MoS_2 Paper

6.2.2 Electrode Study

Electrochemical study has been performed to study the surface properties of modified electrodes using Chronoamperometry. The phenomenon of charge transfer is studied across Bare Whatman filter paper-1, MoS_2/Paper Composite and BSA/Anti-HER-2/MoS_2/Paper Composite as shown in Fig.6.11. It is found that the magnitude of current obtained for MoS_2/Paper Composite immune electrode is ≈1mA. The immobilization of Anti-HER-2 on to the MoS_2/Paper Composite electrode accredited to a decrease in the current response. This decrease may be due to the masking of charge conducting pathways by the globular antibodies. BSA immobilization is then further carried out to block the non-specific sites present at the electrode surface, which resulted to an obvious decrease in the current response of the BSA/Anti-HER-2/MoS_2/Paper Composite immune electrode to 0.55 mA.

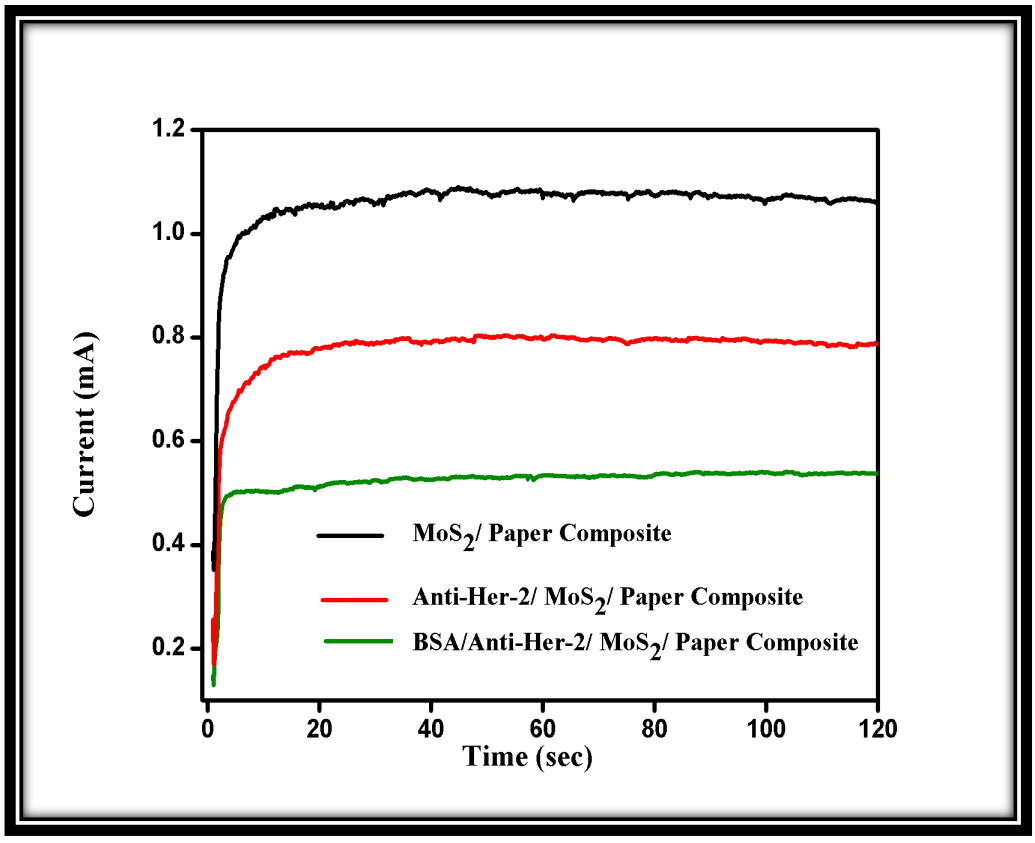

Figure 6.11 Chronoamperometry results of Bare Whatman filter paper-1(Black), MoS_2/Paper Composite (Red) and BSA/Anti-HER-2/MoS_2/Paper Composite immunoelectrode (Green) measured in PBS containing 5 mM $[Fe(CN)_6]^{3-}$ and 0.9% NaCl

6.2.3 pH Study

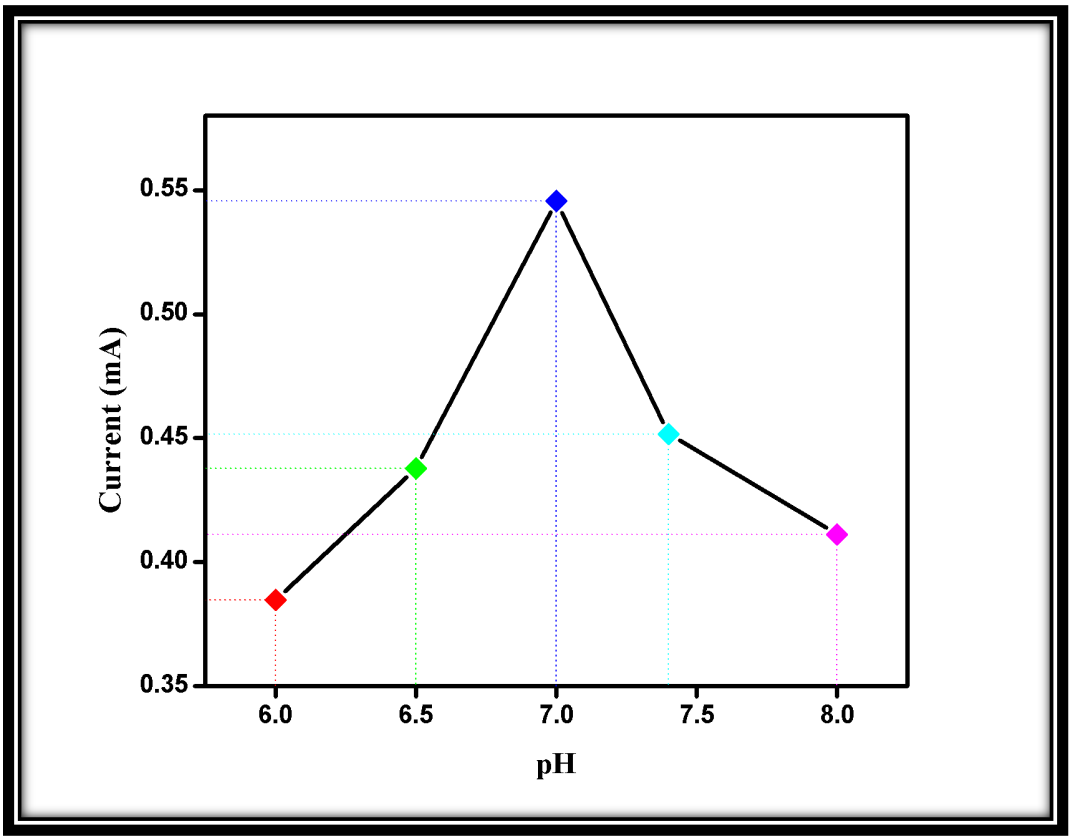

Figure 6.12 Electrochemical response of BSA/Anti-HER-2/MoS_2/Paper Composite immunoelectrode as a function of pH

The electrochemical response of the BSA/Anti-HER-2/MoS2/Paper Composite immunoelectrode was investigated electrochemically in PBS (Phosphate buffer saline) containing $[Fe(CN)6]^{3-/4-}$ at different pH using Chronoamperometry technique. It is found that the maximum current is obtained at pH-7, which signifies that the specific activity of the biological molecules such as enzymes, antibody and antigens is highest at physiological pH. As a result, denaturation of antibody occurs when exposed to slight acidic or basic medium due to the interaction of H^+ or OH^- ions present in the amino acid sequence of antibody. The peak current has been found to increase considerably when pH was increased from 6-7 units and simultaneously the response of the biosensor reduced signifying the reduction in current when the pH is increased further. Thus, for all the electrochemical studies PBS pH-7 was used.

6.2.4 Electrochemcal Response Studies

The change in the electrochemical response of the fabricated BSA/Anti-HER-2/MoS_2 paper based immunosensor with increasing concentration of HER-2 has been analyzed via chronoamperometry in PBS solution containing $[Fe(CN)_6]^{3-/4-}$ (5 mM) and 0.9% NaCl as shown in Figure 6.13 (a). It is observed that increase in the HER-2 concentration results in a corresponding decrease in the peak current of the biosensor. This decrease in the current might be attributed to the interaction of bulky HER-2 molecules with the anti- HER-2 antibodies, resulting in the blocking of charge conduction pathways at the BSA/Anti-HER-2/MoS_2 bio-sensing surface. The corresponding calibration curve revealed the linear dependence of the biosensor's peak current with HER-2 concentration Figure 6.13 (b). The linear range of the biosensor has been found to be 0.1 – 500 ng ml^{-1} which sufficiently covers the entire physiological range of HER-2. The corresponding calibration curve reveals the linear dependence of the biosensor's peak current with HER-2 concentration. In addition, the biosensor displayed an excellent sensitivity of 78 μA mL ng^{-1} cm^{-2} which is found to be much superior to the previously reported biosensors for HER-2 detection. The detection limit, evaluated by 3σ/m, is determined to be 0.07 ng mL^{-1}, where σ is the standard deviation in the electrochemical response and m is the slope (or, sensitivity) of the fabricated BSA/Anti-HER-2/MoS_2 biosensor. Further a control experiment is conducted to determine the electrochemical response of the BSA/Anti-HER-2/MoS_2 immuno electrode as a function of HER-2 concentration (0 – 500 ng ml^{-1}) Fig 6.13 (c). It is found that no significant change in the current response of the BSA/Anti-HER-2/MoS_2 immuno electrode has been found even at higher concentrations of HER-2. It is only attributing to the specificity of antibody-antigen interaction that resulted in the change in the electrochemical response of the BSA/Anti-HER-2/MoS_2 electrode. Thereby, showing the specificity of the electrode. Also, variation in the electrochemical behavior of the as fabricated BSA/Anti-HER-2/MoS_2 immuno electrode in the presence of common interfering agents has also been studied via Chronoamperometry studies Fig 6.13 (d) The response of the biosensor is first recorded in the presence of HER-2

antigen (10 ng ml^{-1}). After that, equal amount of different interferents is added in a sequential manner in their normal physiological range found in serum, such as CEA (10 ng ml^{-1}), cardiac troponin I (cTnI-10 ng ml^{-1}), endothelin-1 (ET-1-10 ng ml^{-1}), CYFRA-21-1(10 ng ml^{-1}) etc. The addition of cTnI as such resulted in no significant change (0 – 0.5%) in the peak response of the fabricated biosensor, while a small change (~ 1%) has been found in the peak response upon addition of remaining interferents. It shows that the as fabricated BSA/Anti-HER-2/MoS_2 electrode remains largely unaffected by the presence of interferents and has got great potential for practical applicability in future.

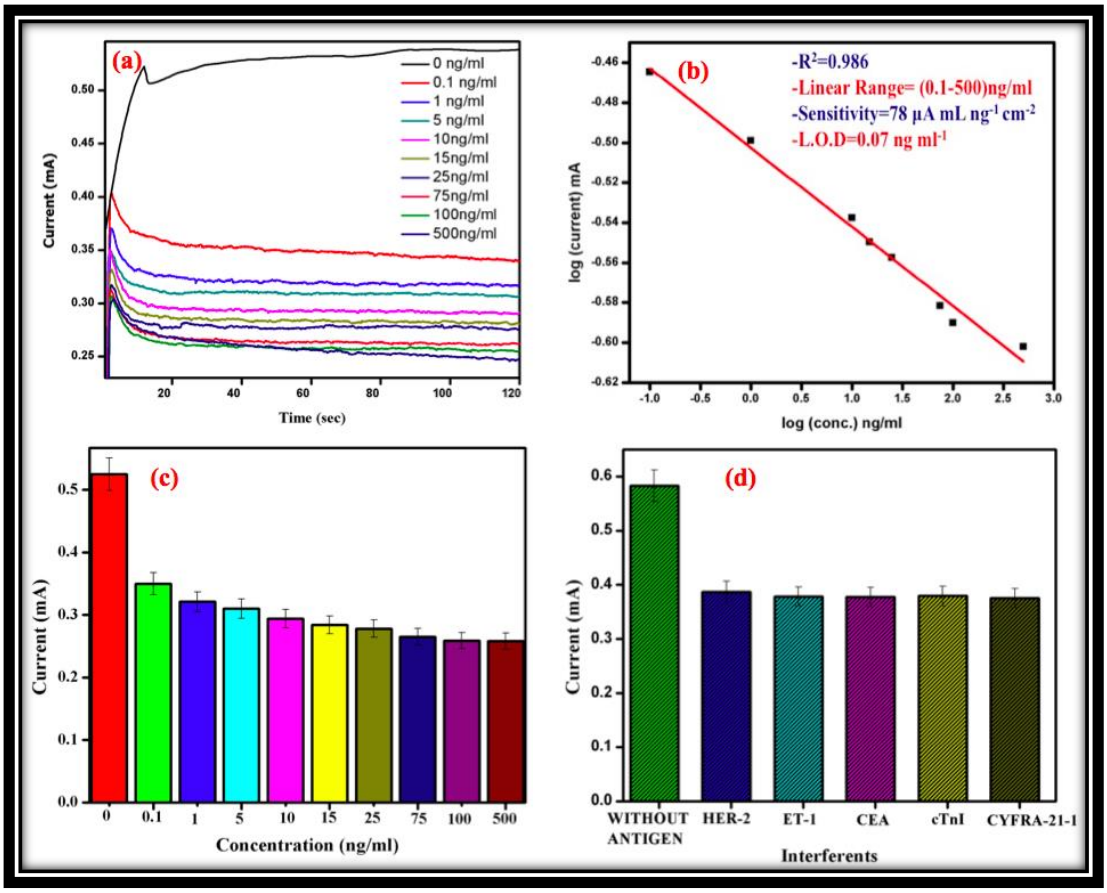

Figure 6.13 (a) Chronoamperometry curves of the BSA/Anti-HER-2/MoS_2/Paper immunoelectrode as a function of HER-2 concentration (0.1-500 ng/ml),

(b) Calibration plot derived from Chronoamperometry curves of the BSA/Anti-HER-2/MoS_2/Paper immunoelectrode as a function of HER-2 concentration (0.1-500 ng/ml)

(c) Electrochemical response of the BSA/Anti-HER-2/MoS_2/Paper immunoelectrode as a function of increasing HER-2 concentration (0.1-500 ng/ml)

(d) Peak current response of the BSA/Anti-HER-2/MoS_2/Paper electrode in the presence of HER-2 (10 ng/ml) and other common interferents found in serum.

6.2.5 Stability and Shelf life studies

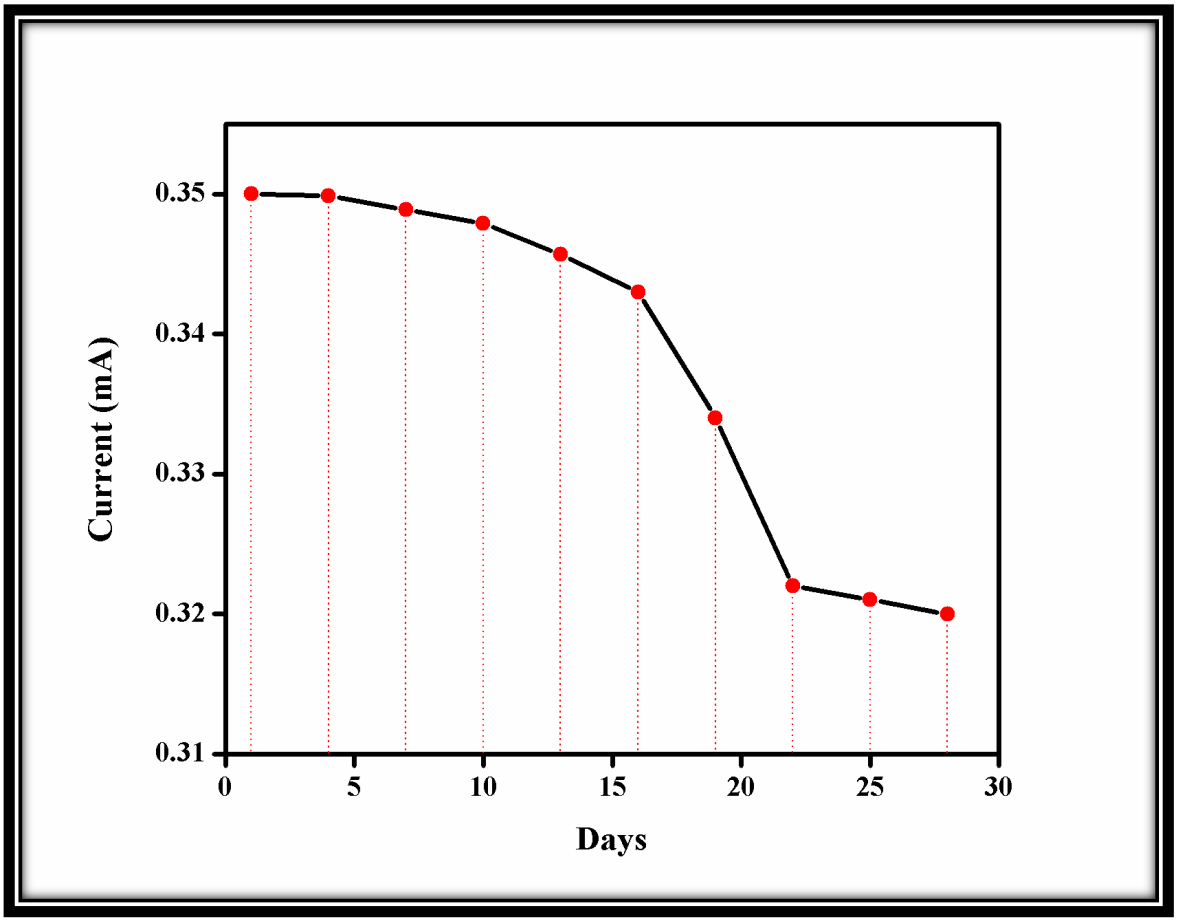

Figure 6.14 The Electrochemical response of MoS_2 / Paper composite electrode measured as a function of time (days)

The stability and shelf life of the fabricated BSA/Anti-HER-2/MoS_2/Paper biosensor has been determined by measuring chronoamperometry response in the presence of standard HER-2 solution (10 ng ml^{-1}) in PBS buffer (at pH 7) containing 5 mM $[Fe(CN)_6]^{3-/4-}$ at a regular interval of five days (Fig. 6.14). It is observed that there is no significant change in electrochemical current upto 20 days after which slight decrease in the current response is observed. The biosensor is found to retain 80% of its original response even after 25 days when stored at 4° C. Further a gradual but continual decrease to less than 30% was observed in less than 25 days thereafter. It shows that the fabricated BSA/Anti-HER-2/MoS_2/Paper exhibits reasonably very good stability for at least 30 days.

6.2.6 Incubation time studies

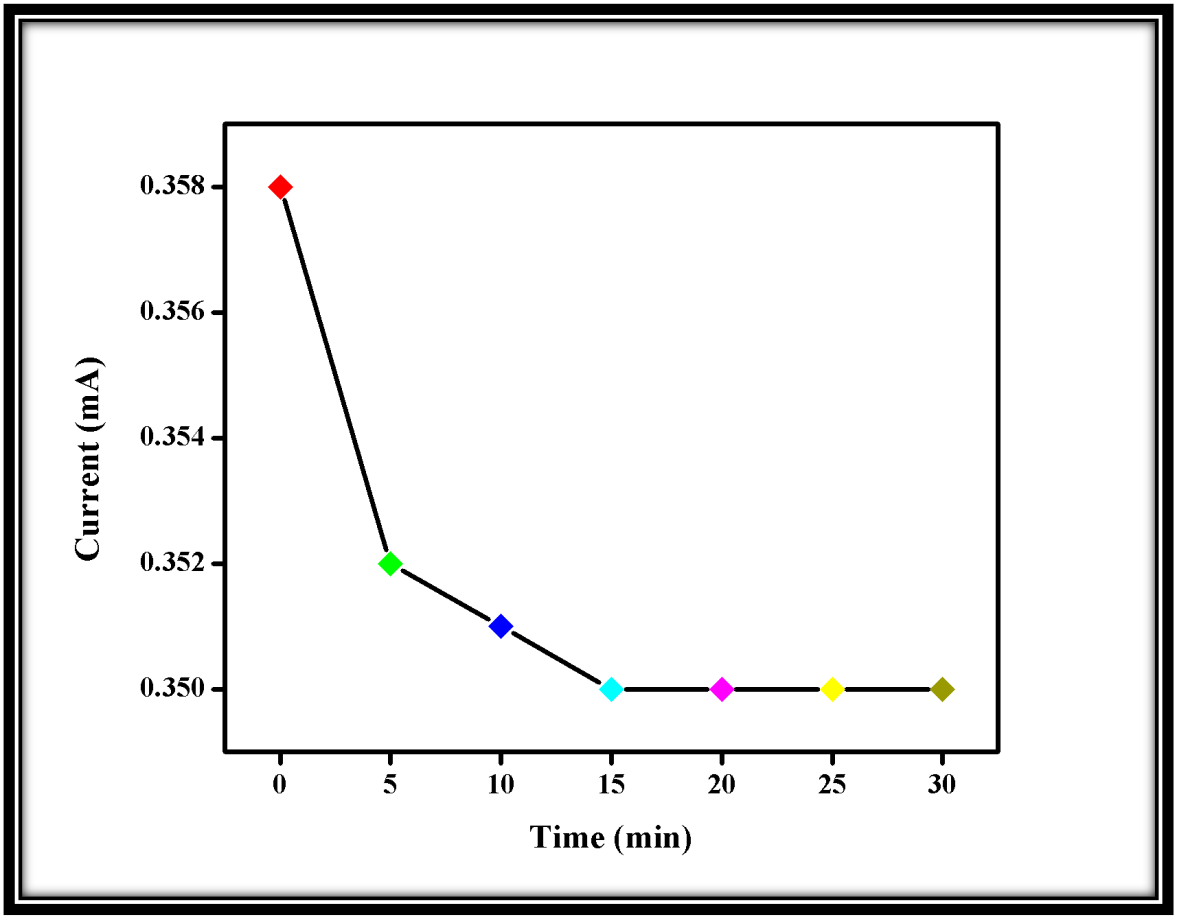

Figure 6.15: The incubation time study of interaction between BSA/Anti-HER-2/MoS_2/Paper immunoelectrode and HER-2

Incubation study has been performed to study the variation of current obtained via Chronoamperometry on interaction of HER-2 with the BSA/Anti-HER-2/MoS_2/Paper immunoelectrode at different incubation times. A decrease in current was obtained with increasing time from 2 to 15 mins. However, after 20 mins of sample incubation the current became nearly constant. Thus, 30 mins is selected as the sample incubation time during which the antigen–antibody reaction reached the steady state.

6.2.7 Flexibility Studies

Figure 6.16 : Optical image of MoS_2/Paper immunoelectrode showing flexible nature

The result of the flexibility studies of MoS_2/Paper composite immunoelectrode has been shown in Fig xyz. The optical image exhibits a greyish black colour image of MoS_2 over paper showing high degree of flexibility. It is observed that no cracks has been seen while bending the paper +180° and -180°. This clearly proves that MoS_2 has got strong hold over the surface of paper to prevent its exfoliation from paper's surface.

6.2.8 Optical images of the conductive and electrochemically active paper

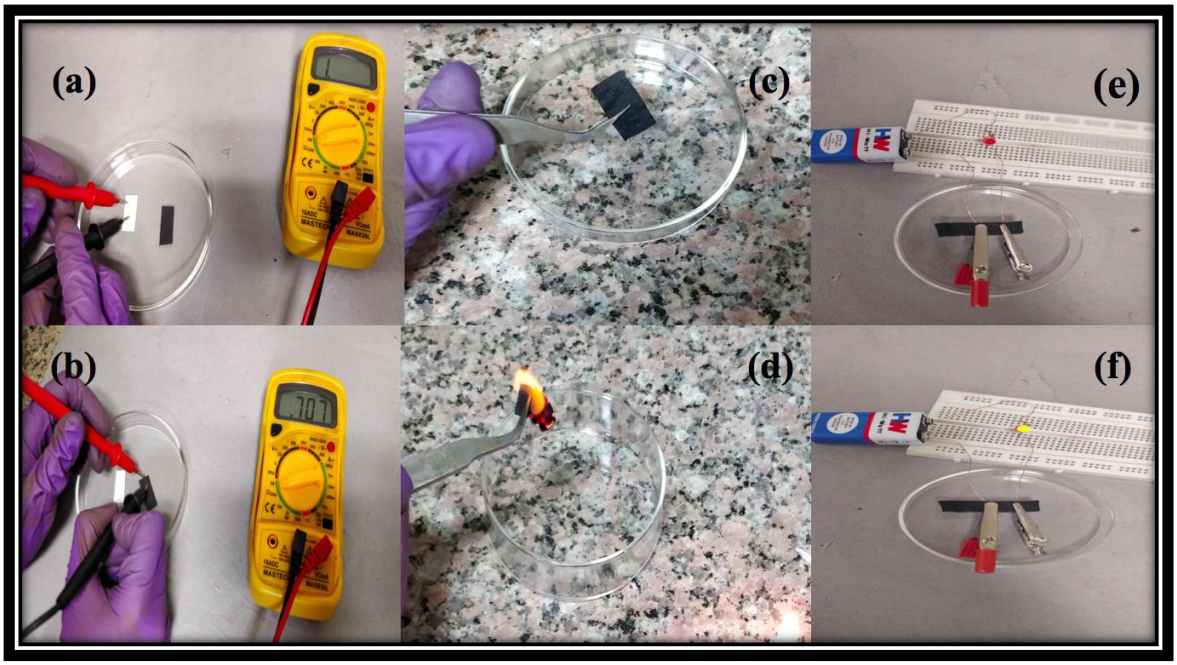

Figure 6.17: Optical image of MoS_2/Paper immunoelectrode showing its optical, disposable and conducting characteristics

Fig.6.17 (a) and (b) Shows optical image of bare and MoS_2/Paper electrode demonstrating multimeter readings. It is seen that this low-cost MoS_2/paper conducting composite platform can be easily decomposed by simple burning or incineration as shown in Fig.6.17 (c) and (d), which is advantageous for electronic, environmental and biomedical waste management systems. Also, the conductivity of the MoS_2/paper electrode can be seen by lighting an LED bulb when current is passed through it a number of times even after folding the conducting paper as shown in Fig.6.17 (e) and (f).

CHAPTER-7

CONCLUSION

In this work, we synthesized an efficient biosensing platform based on cellulose nanocomposite consisting of MoS_2 aggregated nanoflowers for the detection of breast cancer in human blood. The cellulose nanocomposite was synthesized hydrothermally at 180^o C for 20 h. Anti-HER-2 was physisorbed on the surface of electrode and BSA was used for blocking the non-specific sites. The structural investigations of the the BSA/Anti-HER-2/MoS_2 Paper composite were performed using SEM, XRD, FTIR and XPS techniques which corroborated the production of composites with contrasting physicochemical characteristics. A favourable electrochemical response was obtained for the BSA/Anti-HER-2/MoS_2 Paper composite, which showed a 10-fold plus increase in its current over a wide linearity range of (0.1-500) ng ml^{-1} (R^2=0.986). The sensitivity of 78 μA mL ng^{-1} cm^{-2} with a limit of detection of 0.07 ng ml^{-1}, was found to surpass those obtained using several other TMDC-Cellulose based hybrids. Moreover an improved combination of linearity, sensitivity and sensing range reflects on the promise that MoS_2-cellulose composites hold in store as superior paper based POCT devices. Hence, future improvements in the nature of the MoS_2-cellulose composites would be centered on the optimization of substrate characteristics, which could yield a highly reproducible, sensitive, specific, rapid, stable, low cost, flexible and disposable point of care devices.

CHAPTER-8

FUTURE PROSPECTIVES

Owing to the success of the MoS_2-cellulose composites based Conducting Paper in sensing breast cancer levels in serum over a wide linear sensing range, we would like to explore other exciting applications of MoS_2-cellulose composite/nanocomposite in commercially profitable applications like health monitoring and strain sensing. Here, the biosensor shall be a part of a point of care device, which the user will be wearing in the wrist or waist for remote monitoring of the body parameters. Further, emerging applications of MoS_2-cellulose composites are in Point of Care Testing (POCT) devices such as for Sweat sensing by measuring blood lactate and glucose levels in the real time using flexible wearable sensors. Heart rate monitoring can be performed using strains sensors. Here, crucial heart function parameters like Oxygen supply, pulse rate monitoring, CO_2 and O_2 circulation, and breathing frequency can be quantified using the sensing response of the MoS_2-cellulose based flexible, conducting paper. Photodetection studies can be performed in UV and NIR range through strain modulation using PDMS substrate. It has got wide range of applications in the optics and optoelectronics field such as supercapacitors, μpads, LIBs etc. Further, the obtained data can be recorded by a real time monitoring unit consisting of an LED indicator panel and an electronic readout. Then, Bluetooth can be used to establish a wireless connection between the electronic circuitry of the device and the mobile phone of the user. This can be simply achieved by installing an open source Android application on the mobile phone and then the data obtained on the LFM device can be wirelessly transferred to the user's mobile phone. Thus, using this LFM device, the user can be able to diagnose and monitor serious heart conditions before the onset of any abnormal situation, which endanger the life of the individual if left untreated for long. An additional biomedical application of the MoS_2-cellulose composite sensor is as a wearable sensor to monitor the frequency modulation during human motion, which is an important fitness parameter of our body. Hence, this POCT device could be used to

monitor the lung fitness of an individual, who can simply monitor the applied strain at different time intervals post exercise using flexible, wearable devices.

REFERENCES

[1] Tenne R.: 'Core–shell PbI2@WS2 inorganic nanotubes from capil- lary wetting', Nat. Nanotechnol., 2006, 1, pp. 103–11

[2] Tang G.G., Tang H., Li C.S., Li W.J., Ji X.R.: 'Synthesis and charac- terization of flowerlike MoS_2 nanostructures through CTAB-assisted hydrothermal process', Mater. Lett., 2011, 65, pp. 3457–60

[3] Yu H.T., Liu Y., Brock S.L.: 'Synthesis of discrete and dispersible MoS_2 nanocrystals', Inorg. Chem., 2008, 47, pp. 1428–34

[4] Chang K., Chen W.X.: 'Single-layer MoS_2/graphene dispersed in amorphous carbon: towards high electrochemical performances in rechargeable lithium ion batteries', J. Mater. Chem., 2011, 21, pp. 17175–184

[5] Rapoport L., Bilik Y., Feldman Y., Homyonfer M., ET AL.: 'Hollow nanoparticles of WS_2 as potential solid-state lubricants', Nature, 1997, 38, pp. 7791–793

[6] Chhowalla M., Amaratunga G.A.J.: 'Thin films of fullerene-like MoS_2 nanoparticles with ultra-low friction and wear', Nature, 2000, 407, pp. 164–67

[7] Uzcanga I., Bezverkhyy I., Afanasiev P., ET AL.: 'Sonochemical prep- aration of MoS2 in aqueous solution: replication of the cavitation bubbles in an inorganic material morphology', Chem. Mater., 2005, 17, pp. 3575–77

[8] Zelenski C.M., Dorhout P.K.: 'Template synthesis of near- monodisperse1 microscale nanofibers and nanotubules of MoS_2', J. Am. Chem. Soc., 1998, 120, pp. 734–42

[9] Li X.L., Li Y.D.: 'MoS_2 nanostructures: synthesis and electro- chemical Mg^{2+} intercalation', J. Phys. Chem. B, 2004, 108, pp. 13893–900

[10] L. Liang, f. Lan, l. Li, s. Ge, j. Yu, n. Ren, h. Liu and m. Yan, biosensors and bioelectronics, 2016, 86, 756-763.

[11] S. Ge, w. Li, m. Yan, x. Song and j. Yu, journal of materials chemistry b, 2015, 3, 2426-2432.

[12] L. Li, c. Ma, q. Kong, w. Li, y. Zhang, s. Ge, m. Yan and j. Yu, journal of materials chemistry b, 2014, 2, 6669-6674.

[13] F. Lan, G. Sun, L. Liang, S. Ge, M. Yan and J. Yu, Biosensors and Bioelectronics, 2016, 79, 416-422.

[14] C. M. Gao, L. N. Zhang, Y. H. Wang, J. H. Yu and X. R. Song, Biosensors and Bioelectronics, 2016, 83, 327-333.

[15] W. P. Deng, L. Shen, X. Wang, C. L. Yang, J. H. Yu, M. Yan and X. R. Song, Biosensors and Bioelectronics, 2016, 82, 132-139.

[16] G. Sun, H. Yang, Y. Zhang, J. Yu, S. Ge, M. Yan and X. Song, Biosensors and Bioelectronics, 2015, 74, 823-829.

[17] Y. Zhang, L. Ge, M. Li, M. Yan, S. Ge, J. Yu, X. Song and B. Cao, Chemical Communications, 2014, 50, 1417-1419.

[18] L. Li, Y. Zhang, F. Liu, M. Su, L. Liang, S. Ge and J. Yu, Chemical Communications, 2015, 51, 14030-14033.

[19] Y. Wang, J. Xu, C. Ma, S. Li, J. Yu, S. Ge and M. Yan, Journal of Materials Chemistry B, 2014, 2, 3462-3468.

[20] S. Ge, K. Wu, Y. Zhang, M. Yan and J. Yu, Biosensors and Bioelectronics, 2016, 80, 215-221.

[21] G. Sun, L. Zhang, Y. Zhang, H. Yang, C. Ma, S. Ge, M. Yan, J. Yu and X. Song, Biosensors and Bioelectronics, 2015, 71, 30-36.

[22] L. Li, L. Zhang, J. Yu, S. Ge and X. Song, Biosensors and Bioelectronics, 2015, 71, 108-114.

[23] S. Ge, M. Sun, W. Liu, S. Li, X. Wang, C. Chu, M. Yan and J. Yu, Sensors and Actuators B-Chemical, 2014, 192, 317-326.

[24] Y. Zhang, M. Su, L. Ge, S. Ge, J. Yu and X. Song, Carbon, 2013, 57, 22-33.

[25] L. Ge, S. Wang, J. Yu, N. Li, S. Ge and M. Yan, Advanced Functional Materials, 2013, 23, 3115-3123.

[26] S. Wang, L. Ge, L. Li, M. Yan, S. Ge and J. Yu, Biosensors and Bioelectronics, 2013, 50, 262-268.

[27] P. Wang, G. Sun, L. Ge, S. Ge, J. Yu and M. Yan, Analyst, 2013, 138, 4802-4811.

[28] G. Sun, P. Wang, S. Ge, L. Ge, J. Yu and M. Yan, Biosensors and Bioelectronics, 2014, 56, 97-103.

[29] Shizuka Egusa, Shingo Yokota, Kyoko Tanaka, Kei Esaki, Yuri Okutani, Yukiko Ogawa, Takuya Kitaoka, Masahiro Goto and Hiroyuki Wariishi' "Surface modification of a solid-state cellulose matrix with lactose by a surfactant-enveloped enzyme in a nonaqueous medium", J. Mater. Chem., 2009, 19, 1836–1842

[30] Parikshit Sahatiya, S. Solomon Jones, Sushmee Badhulika, "2D MoS_2–carbon quantum dot hybrid based large area, flexible UV–vis–NIR photodetector on paper substrate" Applied Materials Today 10 (2018) 106–114 107

[31] Vinay Khatri, Katalin Halasz, Lidija V. Trandafilovic, Suzana Dimitrijevic´-Brankovic´ , Paritosh Mohanty, Vladimir Djokovic , Levente Csóka, "ZnO-modified cellulose fiber sheets for antibody immobilization" Carbohydrate Polymers 109 (2014) 139–147 April 2014

[32] Zhengyun Wang, Shuang Dong, Mengxi Gui, Muhammad Asif, Wei Wang, Feng Wang, Hongfang Liu, "Graphene paper supported MoS_2 nanocrystals monolayer with Cu submicron-buds: High-performance flexible platform for sensing in sweat", Analytical Biochemistry 543 (2018) 82-89

[33] Kumar S, Kumar S, Tiwari S, Srivastava S, Srivastava M, Yadav BK, Kumar S, Tran TT, Dewan AK, Mulchandani A, Sharma JG. Biofunctionalized nanostructured zirconia for biomedical application: a smart approach for oral cancer detection. Advanced Science. 2015 Aug;2(8):1500048.

[34]Sahatiya P, Puttapati SK, Srikanth VV, Badhulika S. Graphene-based wearable temperature sensor and infrared photodetector on a flexible polyimide substrate. Flexible and Printed Electronics. 2016 Jun 23;1(2):025006.

[35]Kumar S, Kumar S, Srivastava S, Yadav BK, Lee SH, Sharma JG, Doval DC, Malhotra BD. Reduced graphene oxide modified smart conducting paper for cancer biosensor. Biosensors and Bioelectronics. 2015 Nov 15;73:114-22.

[36]Kumar S, Sen A, Kumar S, Augustine S, Yadav BK, Mishra S, Malhotra BD. Polyaniline modified flexible conducting paper for cancer detection. Applied Physics Letters. 2016 May 16;108(20):203702.

[37]Dungchai W, Chailapakul O, Henry CS. Electrochemical detection for paper-based microfluidics. Analytical chemistry. 2009 Jun 1;81(14):5821-6.

[38]He X, Yuan R, Chai Y, Shi Y. A sensitive amperometric immunosensor for carcinoembryonic antigen detection with porous nanogold film and nano-Au/chitosan composite as immobilization matrix. Journal of biochemical and biophysical methods. 2008 Apr 24;70(6):823-9.

[39]Wang Z, Dong S, Gui M, Asif M, Wang W, Wang F, Liu H. Graphene paper supported MoS2 nanocrystals monolayer with Cu submicron-buds: High-performance flexible platform for sensing in sweat. Analytical biochemistry. 2018 Feb 15;543:82-9.

[40]Kuc A, Zibouche N, Heine T. Influence of quantum confinement on the electronic structure of the transition metal sulfide T S 2. Physical Review B. 2011 Jun 30;83(24):245213.

[41] Chu RX, Lin J, Wu CQ, Zheng J, Chen YL, Zhang J, Han RH, Zhang Y, Guo H. Reduced graphene oxide coated porous carbon–sulfur nanofiber as a flexible paper electrode for lithium–sulfur batteries. Nanoscale. 2017;9(26):9129-38.

[42] Kumar TN, Chandrasekaran N, Phani KL. Structural and electronic modification of MoS 2 nanosheets using S-doped carbon for efficient electrocatalysis of the hydrogen evolution reaction. Chemical Communications. 2015;51(24):5052-5.

[43] Zhang Z, Zhao H, Teng Y, Chang X, Xia Q, Li Z, Fang J, Du Z, Świerczek K. Carbon‐Sheathed MoS2 Nanothorns Epitaxially Grown on CNTs: Electrochemical Application for Highly Stable and Ultrafast Lithium Storage. Advanced Energy Materials. 2018 Mar;8(7):1700174.

[44]Barrera D, Wang Q, Lee YJ, Cheng L, Kim MJ, Kim J, Hsu JW. Solution synthesis of few-layer 2H MX 2 (M= Mo, W; X= S, Se). Journal of Materials Chemistry C. 2017;5(11):2859-64

[45]Zhang Z, Zhao H, Teng Y, Chang X, Xia Q, Li Z, Fang J, Du Z, Świerczek K. Lithium‐Ion Batteries: Carbon‐Sheathed MoS2 Nanothorns Epitaxially Grown on CNTs: Electrochemical Application for Highly Stable and Ultrafast Lithium Storage (Adv. Energy Mater. 7/2018). Advanced Energy Materials. 2018 Mar;8(7):1870029.

[46]Yu H, Yu X, Chen Y, Zhang S, Gao P, Li C. A strategy to synergistically increase the number of active edge sites and the conductivity of MoS 2 nanosheets for hydrogen evolution. Nanoscale. 2015;7(19):8731-8.

[47]Mukherjee S, Biswas S, Ghorai A, Midya A, Das S, Ray SK. Tunable Optical and Electrical Transport Properties of Size and Temperature Controlled Polymorph MoS2 Nanocrystals. The Journal of Physical Chemistry C. 2018 May 22.

[48]Qi D, Li S, Chen Y, Huang J. A hierarchical carbon@ TiO2@ MoS2 nanofibrous composite derived from cellulose substance as an anodic material for lithium-ion batteries. Journal of Alloys and Compounds. 2017 Dec 25;728:506-17.

[49]Pan X, Song X, Lin S, Bi K, Hao Y, Du Y, Liu J, Fan D, Wang Y, Lei M. A facile route to graphite-tungsten nitride and graphite-molybdenum nitride nanocomposites and their ORR performances. Ceramics International. 2016 Nov 1;42(14):16017-22.

[50]Chen YY, Zhang Y, Jiang WJ, Zhang X, Dai Z, Wan LJ, Hu JS. Pomegranate-like N, P-doped Mo2C@ C nanospheres as highly active electrocatalysts for alkaline hydrogen evolution. ACS nano. 2016 Sep 14;10(9):8851-60.

[51]Atar N, Eren T, Demirdögen B, Yola ML, Çağlayan MO. Silver, gold, and silver@ gold nanoparticle-anchored l-cysteine-functionalized reduced graphene oxide as electrocatalyst for methanol oxidation. Ionics. 2015 Aug 1;21(8):2285-93.

[52]Liu P, Liu Y, Ye W, Ma J, Gao D. Flower-like N-doped MoS2 for photocatalytic degradation of RhB by visible light irradiation. Nanotechnology. 2016 Apr 25;27(22):225403.

[53]Lin Z, Wang X. Nanostructure engineering and doping of conjugated carbon nitride semiconductors for hydrogen photosynthesis. Angewandte Chemie. 2013 Feb 4;125(6):1779-82.

[54]Kumar NA, Choi HJ, Shin YR, Chang DW, Dai L, Baek JB. Polyaniline-grafted reduced graphene oxide for efficient electrochemical supercapacitors. ACS nano. 2012 Feb 3;6(2):1715-23.

[55]Zhao Y, Ikram M, Zhang J, Kan K, Wu H, Song W, Li L, Shi K. Outstanding gas sensing performance of CuO-CNTs nanocomposite based on asymmetrical schottky junctions. Applied Surface Science. 2018 Jan 15;428:415-21

[56]Yang X, Fu W, Liu W, Hong J, Cai Y, Jin C, Xu M, Wang H, Yang D, Chen H. Engineering crystalline structures of two-dimensional MoS 2 sheets for high-performance organic solar cells. Journal of Materials Chemistry A. 2014;2(21):7727-33.)

[57]Qiao XQ, Hu FC, Tian FY, Hou DF, Li DS. Equilibrium and kinetic studies on MB adsorption by ultrathin 2D MoS 2 nanosheets. Rsc Advances. 2016;6(14):11631-6.

[58]Qiao XQ, Hu FC, Tian FY, Hou DF, Li DS. Equilibrium and kinetic studies on MB adsorption by ultrathin 2D MoS 2 nanosheets. Rsc Advances. 2016;6(14):11631-6.

[59]Li Q, Walter EC, Van der Veer WE, Murray BJ, Newberg JT, Bohannan EW, Switzer JA, Hemminger JC, Penner RM. Molybdenum disulfide nanowires and nanoribbons by electrochemical/chemical synthesis. The Journal of Physical Chemistry B. 2005 Mar 3;109(8):3169-82.

[60]Mann J, Ma Q, Odenthal PM, Isarraraz M, Le D, Preciado E, Barroso D, Yamaguchi K, von Son Palacio G, Nguyen A, Tran T. 2-Dimensional transition metal dichalcogenides with tunable direct band gaps: MoS2 (1–x) Se2x monolayers. Advanced Materials. 2014 Mar;26(9):1399-404.

[61]Wang QH, Kalantar-Zadeh K, Kis A, Coleman JN, Strano MS. Electronics and optoelectronics of two-dimensional transition metal dichalcogenides. Nature nanotechnology. 2012 Nov;7(11):699.

[62]S. Y. Oh, et al., "Crystalline structure analysis of cellulose treated with sodium hydroxide and carbon dioxide by means of X-ray diffraction and FTIR spectroscopy," Carbohydrate research, vol. 340, pp. 2376-2391, 2005.

[63]Vattikuti SV, Byon C. Synthesis and characterization of molybdenum disulfide nanoflowers and nanosheets: nanotribology. Journal of Nanomaterials. 2015 Jan 1;2015:9.

[64]Yang YP, Zhang Y, Lang YX, Yu MH. Structural ATR-IR analysis of cellulose fibers prepared from a NaOH complex aqueous solution. InIOP Conference Series: Materials Science and Engineering 2017 Jun (Vol. 213, No. 1, p. 012039). IOP Publishing.